Optimizing Air-borne Network-in-a-box Deployment for Efficient Remote Coverage

Sidrah Javed, *Member, IEEE*, Yunfei Chen, *Senior Member, IEEE*,
Mohamed-Slim Alouini, *Fellow, IEEE*, and Cheng-Xiang Wang, *Fellow, IEEE*

***Abstract*—Among many envisaged drivers for sixth generation (6G), one is from the United Nation's Sustainability Development Goals 2030 to eliminate digital inequality. Remote coverage in sparsely populated areas, difficult terrains or emergency scenarios requires on-demand access and flexible deployment with minimal capex and opex. In this context, network-in-a-box (NIB) is an exciting solution which packs the whole wireless network into a single portable and re-configurable box to support multiple access technologies such as WiFi/2G/3G/4G/5G etc. In this paper, we propose low-altitude platform station (LAPS) based NIBs with stratospheric high-altitude platform station high-altitude platform station (HAPS) as backhaul. Specifically, backhaul employs non-orthogonal multiple access (NOMA) with superposition coding at the transmitting HAPS and successive interference cancellation (SIC) at the receiving NIBs, whereas the access link (AL) employs superposition coding along with the regularized zero-forcing (RZF) precoding at the NIB in order to elevate the computational overhead from the ground users. The required number of airborne NIBs to serve a desired coverage area, their optimal placement, user association, beam optimization, and resource allocation are optimized by maximizing the sum-rate of the AL while maintaining the quality of service. Our findings reveal the significance of thorough system planning and communication parameters optimization for enhanced system performance and best coverage under limited resources.**

***Index Terms*—HAPS, non-orthogonal multiple access, network-in-a-box, unmanned aerial vehicles, and 6G.**

I. Introduction

The upcoming generations of wireless communications envision a comprehensive network capable of delivering ubiquitous and resilient connections to eliminate the digital divide [1]–[3]. The emerging technologies, such as aerial communications, have the potential to reach the unconnected people in remote areas. These platforms, such as drones, balloons, aircrafts, and airships, offer unique advantages that can overcome limitations of traditional terrestrial and satellite communications [4], [5]. For instance, aerial platforms offer flexible deployment rendering rapid on-demand coverage with mobility in remote or disaster-affected areas [6], [7]. Moreover, they are promising candidates for extensive coverage to reach communities in geographically challenging locations. In addition, they may be less susceptible to disruption caused by natural disasters compared with ground-based infrastructure. These features make aerial communications a valuable tool for connecting unserved or underserved populations. They can function synergistically with the existing ground and space infrastructure [8], thereby bridging the digital divide and connecting the unconnected.

In aerial communications, multiple platforms can be combined in multi-layer, where LAPS can offer access link (AL) to the ground user (GU)s whereas HAPS provides the backhaul link (BL) to all the serving LAPS. HAPS can be implemented in the form of airship, aircraft or tethered balloons, while, LAPS can be realized as unmanned aerial vehicle (UAV)s. Although HAPS are capable of directly connecting to the GUs using 4G LTE or 5G NR [9], but, the spectrum compatible with the existing GU equipment offers low throughput. On the other hand, employing LAPS as an intermediate layer between HAPS and GUs can increase the overall system throughput by allowing the use of higher frequency bands for backhaul and higher area throughput of LAPS.

The communications networks using aerial platforms must be adaptive and seamlessly integrable. In this context, NIB (portable network or pop-out network) emerges as a multi-standard 2G/3G/4G/5G all-in-one, rapidly deployable hardware and software solution in a compact and portable unit [10]. NIB generally consists of eNodeB, evolved packet core (EPC), content server, and an optional IP multimedia subsystem (IMS) [11]. It can provide connectivity for a group of devices, allowing them to communicate with each other via text messages, calls or video services. The salient features of NIBs that motivated us to employ it for remote coverage include on-demand coverage, flexible deployment, plug-and-play, dynamic configuration, adaptability, scalability, and seamless inter-operability. NIBs portability enables it to qualify as a "bring-your-own-coverage" solution. The compact reconfigurable package can allow its function as base station to support multiple radio access technologies (RATs). With efficient size, weight, and power (SWaP) characteristics, NIBs can also be the building blocks of flexible and adaptable networks [12]. NIBs render widespread applications in commercial, government, and private sectors for remote coverage, disaster relief, or enhanced cyber security [13], [14]. They can offer emergency services when public infrastructure is compromised but the quality/timings of services are critical. In addition, they provide practical, affordable, and portable solution for on-demand coverage in remote/hard-to-reach areas in challenging contexts. This is beneficial for the tactical and enterprise networks [15]. Similarly, NIB technology can be used for service provisioning to end users using multiple radio interfaces and/or to extend the wireless backhaul connectivity to the external network. It can either function as a stand-alone network or as part of other legacy networks. It can also be used

S. Javed and Y. Chen are with the Department of Engineering, University of Durham, DH1 3LE, England. E-mail: {sidrah.javed, yunfei.chen} @durham.ac.uk, M.S. Alouini is with CEMSE Division, King Abdullah University of Science and Technology (KAUST), Thuwal, Makkah Province,23955-6900 Saudi Arabia. E-mail:slim.alouini@kaust.edu.sa, and C.-X. Wang is with the National Mobile Communications Research Laboratory, School of Information Science and Engineering, Southeast University, Nanjing 211189, China. E-mail: chxwang@seu.edu.cn.

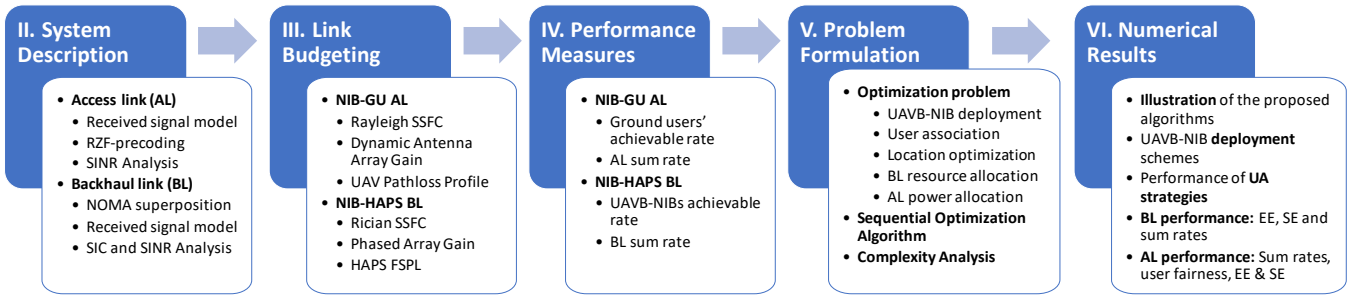

Fig. 1: Paper Outline

as a edge computing server to reduce the transmission delays and minimize traffic on the backhaul links [15]. Therefore, NIB can play a crucial role in the internet of things (IoT).

The concept of a small portable network with few physical devices was conceived in the preliminary works in [16] and [17]. NIBs can either operate as a stand-alone network or co-exist with an exiting network. In this regard, Huang et al. [18] proposed a physical device that connects to the pre-existent base stations in order to restore the original mobile network. The stand-alone NIB-based network was investigated to support smart health IoT services and broadband services in rural areas [19]. Recently, an efficient online service function chain deployment algorithm was proposed for dynamic network function virtualization in NIBs for industrial applications [20]. Likewise, 6G-enabled NIB's channel characteristics were explored for the internet of connected vehicles to realize full-coverage, full-spectrum, and full applications [21]. Another industrial application was the secure decentralized spatial crowd-sourcing for 6G-enabled NIBs, which enabled the collection/transmission of security information on the blockchain using NIB, without depending on the third party [22]. Moreover, EmergeNet provided reliable and repidly deployable small-scale cellular network for emergency and disaster scenariosx which was based on self-organizing network to enable autonomous decision-making for optimal network functioning [23]. NIBs were used for remote coverage and emergency deployment owing to their cost effective design and deployment [24].

None of the existing works has studied the deployment issue of NIB. However, this is important for its efficient operation. In this paper, we jointly address the NIB deployment, resource allocation, service provisioning, and backhauling challenges. In this context, multiple UAVB-NIBs hover over the area of interest where each UAVB-NIB is equipped with downward facing antenna arrays for communication with GUs and upward facing antenna for connection with the HAPs. Highly directional antenna at UAVB-NIBs is used for BL so that it can direct beam to HAPS mitigating the free-space path losses (FSPL). For backhaul, HAPS employs NOMA to serve different UAVB-NIBs that share the same spectral and temporal resources. In addition, each UAVB-NIB employs RZF precoding for GUs accessing same RAT in its coverage area. A holistic approach and suitable algorithms to tackle the aforementioned challenges while guaranteeing user's QoS, fairness, energy, and spectral efficiency are proposed. This work presents a novel sequential algorithm that can solve the problems of deployment, user association (UA), beam optimization and resource allocation to maximize the system performance with limited power, spectrum and time resources. The main contributions of this work are:

- Deployment problem is solved using Geometric Disk Cover (GDC) algorithm which determines the minimum number of required UAVB-NIBs and their locations. Moreover, the UA problem is resolved using greedy algorithm with the objective to maximize the SINR. Each user is served by one and only one spot beam for user fairness (UF) and interference mitigation.
- After the UA, UAVB-NIBs location optimization is conducted to minimize beam-width/beam-radius to serve the associated users. The reduced beamwidth renders directive beam with high power density and antenna gain.
- For backhaul, HAPS employs phased antenna arrays and NOMA scheme to serve all the UAVB-NIBs in its coverage area [25]. The closed-form solution to the NOMA power allocation problem is presented.
- For AL, we employ successive convex approximation (SCA) to iteratively allocate power to different RAT users with the target to maximize the achievable sum rate under QoS constraints and backhaul limitations.
- The achievable data rate, energy efficiency (EE), spectral efficiency (SE) and UF of the proposed system are investigated to quantify the performance gains of the proposed algorithms over the existing ones.

The rest of the paper is organized as follows and also shown in Fig. 1: Section II describes the detailed system model for the communication between HAPS to UAVB-NIBs and between UAVB-NIBs and the GUs. Section III details the propagation model and link budget to incorporate both small-scale and large-scale fading effects in the access and backhaul channel. Next, achievable sum rates for the access and BLs are determined in Section IV. Subsequently, Section V formulates and solves the optimization problem. Numerical results are illustrated in Section VI followed by the conclusions and acknowledgments in Section VII and VIII, respectively. The most frequently used symbols in the paper are summarized in Table I for the reader's convenience.

II. System Description

In order to offer aerial coverage to a remote circular area of radius R having K GUs with coordinates $u_k \in \mathbb{R}^2 \ \forall k$ (on the horizontal plane), NIBs are mounted on UAVs for

TABLE I: Most frequently used symbols

Total coverage radius	R	Total ground users	K
UAVB-NIB coverage radius	r_j	HAPS beam center	$\mathbf{c}_0$
Total UAVB-NIBs	J	GUs horizontal coordinates	$\mathbf{u}_k$
UAVB-NIB altitude	H_j	UAVB-NIB ground location	$\mathbf{c}_j$
UAVB-NIB transmit antennas	M	Jain's Fairness Index	$\mathcal{J}$
Radio access technology	Ω	Precoding vector	$\mathbf{w}_{kj}^{\Omega}$
User association parameter	α_k^j	Channel b/w GU and UAVB-NIB	$\mathbf{h}_{kj}^{\Omega}$
RAT operation indicator	β_k^{Ω}	Transmit signal for user k	s_{kj}^{Ω}
UAVB-NIB power budget	P_j^{Ω}	Power factor for user k	p_{kj}^{Ω}
Ground user received signal	y_{kj}^{Ω}	Thermal noise	n_{kj}^{Ω}
AL Channel Matrix	$\mathbf{H}_j^{\Omega}$	Precoding Matrix	$\mathbf{W}_j^{\Omega}$
Regularization scalar	ω	Normalization scalar	ζ_j^{Ω}
Identity Matrix	$\mathbf{I}_M$	Received SINR at GU	γ_{kj}^{Ω}
Noise variance	σ_{kj}^{Ω}	Transmit SNR	$\bar{\gamma}_{kj}^{\Omega}$
HAPS transmit power	P_H	Power factor for UAVB-NIB j	f_j
Received UAVB-NIB signal	v_j	Information signal for UAVB-NIB j	x_j
UAVB-NIB Elevation Angle	ϕ_{jk}	UAVB-NIB One-sided HPBW	$\theta_j^{3\text{dB}}$
UAVB-NIB received SINR	Γ_j	GU Offset angle	θ_{jk}
HAPS Channel bandwidth	B_H	Distance of GU from UAVB-NIB	d_{jk}
UAVB-NIB thermal noise	z_j	Noise figure	NF_k
UAVB-NIB Transmit antenna gain	G_{jk}^{Ω}	FSPL b/w GU and UAVB-NIB	L_{jk}^{Ω}
Maximum beam gain	$G_{\max}$	First-kind Bessel function Order-n	$\mathcal{J}_n$
Channel components variance	ϑ	Speed of light	S_L
LOS parameter	η_{LOS}	NLOS parameter	η_{NLOS}
Carrier frequency	f_c^{Ω}	Decibel	[dB]
AL SSFC	$\tilde{h}_{kj}^{\Omega}$	BL SSFC	$\tilde{g}_j$
HAPS Transmit antenna gain	G_j^{HAPS}	FSPL b/w HAPS and UAVB-NIB	L_j^{HAPS}
HAPS peak antenna gain	G_0^{HAPS}	Minimum required user rate	$R_{\min}$
Angle of departure of UAVB-NIB	ψ_j	HAPS HPBW	$\theta_{\text{HAPS}}^{3\text{dB}}$
Carrier wavelength of HAPS	λ	Distance of UAVB-NIB from HAPS	d_j
Achievable rate of k^{th} user	R_{kj}^{Ω}	Sum rate of the AL	R_a
Achievable rate of j^{th} UAVB-NIB	R_j	Sum rate of the BL	R_b
Circuit power consumption in AL	P_{c_1}	Circuit power consumption in BL	P_{c_2}
Achievable rate of l^{th} UAVB-NIB to decode j^{th} UAVB-NIB's message			$R_{j\to l}$
Channel bandwidth allocation by j^{th} UAVB-NIB			B_j^{Ω}
Channel coefficient b/w user k and UAVB-NIB j			h_{kj}^{Ω}
Channel coefficient b/w HAPS and UAVB-NIB j			g_j
Channel Coefficient b/w HAPS and UAVB-NIB			g_j
Set of GUs associated with j^{th} UAVB-NIB			K_j
Parameters for the link b/w user k and UAVB-NIB j operating at RAT Ω			$\square_{kj}^{\Omega}$

quick deployment. The coverage is offered by a fleet of J UAVB-NIBs, each hovering at an altitude H_j and covering a circular ground area with center $\mathbf{c}_j$ and 2D horizontal radius r_j where $j \in \{1, 2, \ldots, J\}$, as shown in Fig 2. Each cell is served by a highly-directional and flexible beam from UAVB-NIB, using down-facing M antennas, allowing frequency reuse in the neighboring cells for efficient spectrum allocation and minimal interference. We employ software-defined network based NIB where each NIB j is capable of operating at various RATs $\Omega \in \{\text{WiFi, 3G, 4G, 5G}\}$ to serve K_j^{Ω} compatible users distributed uniformly in its coverage area. The number of users demanding RAT Ω follows the probability mass function Pr_{Ω}. We use the association parameters $\alpha_k^j \in \{0, 1\}$ and $\beta_k^{\Omega} \in \{0, 1\}$ to indicate that the user k is associated with j^{th} UAVB-NIB operating at RAT Ω, respectively, at a given time. We restrict $\sum_j \alpha_k^j = 1 \; \forall \; k$ for UF and $\sum_{\Omega} \beta_k^{\Omega} = 1 \; \forall \; k$ for effective resource allocation. The received signal at user k from j^{th} NIB operating at RAT Ω is given by:

$$y_{kj}^{\Omega} = \mathbf{h}_{kj}^{\Omega H} \mathbf{w}_{kj}^{\Omega} \alpha_k^j \beta_k^{\Omega} \sqrt{p_{kj}^{\Omega} P_j^{\Omega}} s_{kj}^{\Omega} + \sum_{\substack{l=1 \\ l \neq k}}^{K} \mathbf{h}_{kj}^{\Omega H} \mathbf{w}_{lj}^{\Omega} \alpha_l^j \beta_l^{\Omega} \sqrt{p_{lj}^{\Omega} P_j^{\Omega}} s_{lj}^{\Omega} + n_{kj}^{\Omega}, \quad (1)$$

where $\mathbf{h}_{kj}^{\Omega} \in \mathbb{C}^M$ is the channel vector between M antennas of j^{th} NIB and the single-antenna user k operating at RAT Ω, whereas $\mathbf{w}_{kj}^{\Omega} \in \mathbb{C}^M$ is the pre-coding vector for user k. Moreover, $p_{kj}^{\Omega} \in \mathbb{R}$ and $s_{kj}^{\Omega} \sim \mathcal{CN}(0, 1)$ are the allocated power coefficient and information bearing transmit signal for user k from NIB j on RAT Ω. Furthermore, P_j^{Ω} is the total transmission power budget of NIB j for RAT Ω. One has

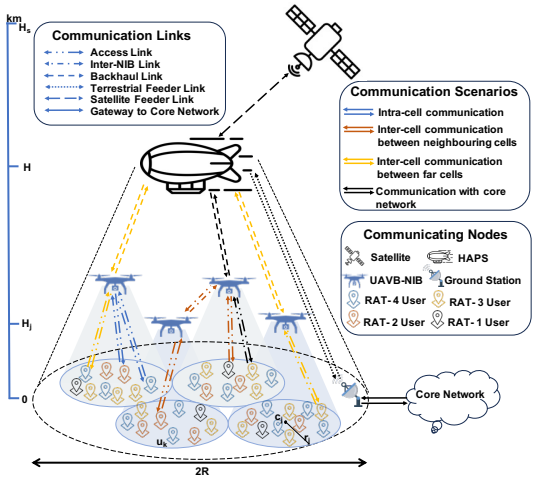

Fig. 2: NIB-based Aerial Communication System

$\sum_k \alpha_k^j \beta_k^{\Omega} p_{kj}^{\Omega} = 1$ for all users in j^{th} cell using RAT Ω to ensure the expenses are within the available power budget. In addition, the receiver thermal noise is modeled as a circular symmetric complex Gaussian random variable, i.e., $n_{kj}^{\Omega} \sim \mathcal{CN}(0, \sigma_{kj}^{\Omega 2})$. Let's define $\mathbf{H}_j^{\Omega} = \left[\mathbf{h}_{1j}^{\Omega}, \mathbf{h}_{2j}^{\Omega}, \ldots, \mathbf{h}_{K_j j}^{\Omega}\right] \in \mathbb{C}^{M \text{x} K_j}$ as the channel matrix comprising of channel coefficients between M transmit antennas of j^{th} UAVB-NIB operating at RAT Ω and the K_j associated users whereas $\mathbf{W}_j^{\Omega} = \left[\mathbf{w}_{1j}^{\Omega}, \mathbf{w}_{2j}^{\Omega}, \ldots, \mathbf{w}_{K_j j}^{\Omega}\right] \in \mathbb{C}^{M \text{x} K_j}$ being the precoding matrix for all connected users, such that the $\mathbf{w}_{kj}^{\Omega}$ intended for user k is orthogonal to every channel vector $\mathbf{h}_{lj}^{\Omega}$ associated with users $l \neq k$. Then, the received signal vector can be written as $\mathbf{y} = \mathbf{H}_j^{\Omega H} \mathbf{W}_j^{\Omega} \mathbf{x} + \mathbf{n}$, where $\mathbf{x}$ and $\mathbf{n}$ are the input signal vector and thermal noise vector at the receiver, respectively, with entries $\alpha_k^j \beta_k^{\Omega} \sqrt{p_{kj}^{\Omega} P_j^{\Omega}} s_{kj}^{\Omega}$ and n_{kj}^{Ω} for all associated users with j^{th} UAVB-NIB which are operating at RAT Ω. Therefore, the RZF pre-coder can be determined as [26]

$$\mathbf{W}_j^{\Omega} = \zeta_j^{\Omega} (\mathbf{H}_j^{\Omega} \mathbf{H}_j^{\Omega H} + \omega \mathbf{I}_M)^{-1} \mathbf{H}_j^{\Omega}, \quad (2)$$

where ω is the regularization scalar and ζ_j is the normalization scalar satisfying

$$\zeta_j^{\Omega 2} = \frac{1}{\text{tr}[(\mathbf{H}_j^{\Omega} \mathbf{H}_j^{\Omega H} + \omega \mathbf{I}_M)^{-1} \mathbf{H}_j^{\Omega} \mathbf{H}_j^{\Omega H} (\mathbf{H}_j^{\Omega} \mathbf{H}_j^{\Omega H} + \omega \mathbf{I}_M)^{-1}]}. \quad (3)$$

It is important to note that user k will only experience co-channel interference from users operating at the same RAT located within the same UAVB-NIB coverage area/cell. There is no inter-RAT interference as they operate at different frequency bands. Thus, the SINR γ_{kj}^{Ω} of the received signal y_{kj}^{Ω} can be derived as

$$\gamma_{kj}^{\Omega} = \frac{|\mathbf{h}_{kj}^{\Omega H} \mathbf{w}_{kj}^{\Omega}|^2 \alpha_k^j \beta_k^{\Omega} p_{kj}^{\Omega}}{\sum_{\substack{l=1 \\ l \neq k}}^{K} |\mathbf{h}_{kj}^{\Omega H} \mathbf{w}_{lj}^{\Omega}|^2 \alpha_l^j \beta_l^{\Omega} p_{lj}^{\Omega} + (\bar{\gamma}_{kj}^{\Omega})^{-1}}, \quad (4)$$

where, $\bar{\gamma}_{kj}^{\Omega} = P_j^{\Omega} / \sigma_{kj}^{\Omega 2}$ is the transmit SNR with noise variance $\sigma_{kj}^{\Omega 2}(\text{dBm}) = -174 + 10 \log(B_j^{\Omega}) + \text{NF}_\text{k}$. Here, B_j^{Ω} depicts the allocated channel bandwidth by j^{th} UAVB-NIB for RAT Ω and NF_k denotes the noise figure of the k^{th} user [27].

Fig. 2 illustrates different communication scenarios in the AL: Scenario I is the intra-cell communication within the UAVB-NIB coverage area, Scenario II is the inter-cell communication between GUs through the neighboring NIBs, Scenario III is the inter-cell communication of GUs between distant UAVB-NIBs, and Scenario IV is the communication with core network. Interestingly, the NIB base stations are capable of independent routing and communicating in Scenarios I and II, whereas in Scenarios III and IV the communication is carried through the BL.

For the backhaul, consider a typical unmanned solar-powered quasi-stationary HAPS at an altitude H over the desired coverage area with radius R ranging between 60km-400km. The HAPS operates from the stratospheric location (preferably between 18km-24km), pertaining to the suitable atmospheric conditions for the stable flight operation. HAPS provides BLs to J UAVB-NIBs over the fourth-generation (4G) long-term evolution (LTE) or 5G new radio (NR) air interfaces. It can further be connected to the terrestrial or satellite gateway through the RF feeder link [9] or free-space optical communication link [28]. HAPS communication panel employs phased antenna arrays to fixate the coverage relative to the station-keeping flight pattern. Within the coverage area, the channel gain varies by increasing the distance from the beam center. The strongest channel gain is available along the boresight direction. However, as the distance varies and/or the azimuth direction deviates from the boresight, the performance can be degraded due to the increased path loss and reduced antenna radiation pattern gain. The striking difference in the channel gains of the connected UAVB-NIBs enables us to reap maximum benefits offered by non-orthogonal multiple access (NOMA). Considering the DL-NOMA scenario, where the UAVB-NIBs are served by a directional beam with superposition coding as [1]

$$\bar{x} = \sum_{j=1}^{J} \sqrt{f_j P_H} x_j, \tag{5}$$

where P_H is the available power budget for transmission after deducting the aerodynamics, electronics, and night-time operational expenses from the available solar power at a given time [29]. Moreover, f_j and x_j are the fraction of power allocated to and intended information signal for the j^{th} UAVB-NIB, respectively. It is important to highlight that $\sum_{j=1}^{J} f_j \leq 1$ in order to limit the power division within given budget. Thus, using conventional wireless communication model, the received signal at j^{th} NIB from the HAPS is given by

$$v_j = g_j \sqrt{f_j P_H} x_j + g_j \sum_{\substack{i=1 \\ i \neq j}}^{J} \sqrt{f_i P_H} x_i + z_j, \tag{6}$$

where, g_j is the channel gain coefficient between the HAPS array panel and j^{th} UAVB-NIB and z_j is the receiver thermal noise modeled as circular symmetric complex Gaussian random variable, i.e., $z_j \sim \mathcal{CN}(0, \sigma_j^2)$. Clearly, the j^{th} NIB receives the superposed signal and retrieves its own signal using the ordered arrangement $j_1, j_2, \ldots, j_J$ depending on their increasing channel strengths. UAVB-NIB performs SIC by first decoding the information from NIB 1 to $j-1$ and then subtracting it from the received signal. Thus, it can decode its own signal from the resultant by considering the interference from $j+1$ to J as noise. Therefore, the signal-to-interference noise ratio Γ_j for the HAPS-NIB link at the j^{th} UAVB-NIB is given by

$$\Gamma_j = \frac{|g_j|^2 f_j P_H}{|g_j|^2 P_H \sum_{i=j+1}^{J} f_i + \sigma_j^2}, \tag{7}$$

whereas, the NIB with the strongest channel gain can successfully decode the information of all other UAVB-NIBs, rendering the SINR

$$\Gamma_J = \frac{|g_J|^2 f_J P_H}{\sigma_J^2}, \tag{8}$$

where the noise power is given as

$$\sigma_j^2(\text{dBm}) = -174 + 10\log(B_H) + \text{NF}_j, \tag{9}$$

with NF_j denoting the noise figure of the j^{th} NIB [27] and B_H depicting the HAPS channel bandwidth of the BL. It is noteworthy that this work focuses on the downlink communications from HAPS to UAVB-NIBs and then from UAVB-NIBs to GUs. The uplink communication is reciprocal of the downlink communication, however, it will have an additional constraint to bound the transmit data-rate of the associated users according to the backhaul capacity limit, in order to avoid the delays at NIBs.

III. Link Budget

In the aerial communication system, the radio signal propagation from aerial platform undergoes both small-scale and large-scale multipath fading. Moreover, the link channel gain is also dependent on the transmitter antenna gain and the receiver position. In this section, we will carry out link budgeting to model the propagation loss for both HAPS-NIB and NIB-GU links.

A. NIB-GU AL

The link between the UAVB-NIBs and GUs experiences FSPL and multipath fading due to the vertical distance between them and obstacles around the UE, respectively. Thus, each channel coefficient h_{kj}^{Ω} in the channel vector $\mathbf{h}_{kj}^{\Omega}$ can be expressed as:

$$|h_{kj}^{\Omega}|^2 = \frac{|\tilde{h}_{kj}^{\Omega}|^2 G_{jk}^{\Omega}}{L_{jk}^{\Omega}}, \tag{10}$$

where $\tilde{h}_{kj}^{\Omega}$ is the small-scale fading coefficient (SSFC) between the j^{th} UAVB-NIB and k^{th} user operating at RAT Ω. The AL is assumed to be non-LOS dominant and hence $|\tilde{h}_{kj}^{\Omega}|$ is modeled as a Rayleigh distribution with scale parameter $\mho$ having independently and identically normal distributed real and imaginary components i.e., $\Re\{\tilde{h}_{kj}^{\Omega}\} \sim \mathcal{N}(0, \mho^2)$ and $\Im\{\tilde{h}_{kj}^{\Omega}\} \sim \mathcal{N}(0, \mho^2)$. The probability density function of the Rayleigh distribution is well-known to be

$$f(x \mid \mho) = \frac{x}{\mho^2} \exp\left(\frac{-x^2}{\mho^2}\right), \quad x \geq 0 \tag{11}$$

Moreover, UAVB-NIB employs antenna arrays so as to generate a single high-gain dynamic beam and the beam gain from the j^{th} NIB to user k is given by G_{jk}^{Ω} which is mainly determined by the off-axis angle between the GU and the main

[1]The transmitted/received signals, channel gains and allocated powers are function of time. However, the time notation is omitted for brevity.

lobe direction of the UAVB-NIB beam [30]

$$G_{jk}^{\Omega} = G_{\max}\left(\frac{\mathcal{J}_1(\mu_{jk})}{2\mu_{jk}} + 36\frac{\mathcal{J}_3(\mu_{jk})}{(\mu_{jk})^3}\right)^2, \quad (12)$$

where $G_{\max}$ is the maximum beam gain along the boresight direction whereas $\mathcal{J}_1$ and $\mathcal{J}_3$ are the first-kind Bessel functions of order 1 and 3, respectively, and

$$\mu_{jk} = \frac{2.07123\sin\theta_{jk}}{\sin\theta_j^{3\text{dB}}}, \quad (13)$$

with $\theta_j^{3\text{dB}}$ representing the one-sided half-power beam width of j^{th} UAVB-NIB transmit antenna and θ_{jk} marking the offset angle of user k from the beam center. This allows on-demand dynamic beam as per the user distribution, which improves coverage efficiency. In addition, L_{jk}^{Ω} in (10) is the path loss as a function of the distance between j^{th} UAVB-NIB and k^{th} user operating at RAT Ω as [31]:

$$L_{jk}^{\Omega}[\text{dB}] = \frac{\eta_{\text{LOS}} - \eta_{\text{NLOS}}}{1 + a\exp\left(-b(\phi_{jk} - a)\right)} + A_{jk}^{\Omega}, \quad (14)$$

where

$$A_{jk}^{\Omega} = 20\log_{10}(d_{jk}) + 20\log_{10}\left(\frac{4\pi f_c^{\Omega}}{S_L}\right) + \eta_{\text{NLOS}}, \quad (15)$$

$$\phi_{jk} = \arcsin\left(\frac{H_j}{d_{jk}}\right), \quad (16)$$

with $\eta_{\text{LOS}}, \eta_{\text{NLOS}}, a$, and b denoting the constant environment-related parameters while ϕ_{jk}, S_L, f_c^{Ω} and d_{jk} denote the elevation angle of user k from UAVB-NIB j, speed of light, carrier frequency of RAT Ω and distance between the user k and UAVB-NIB j. Consequently, the linear pathloss in (10) is $L_{jk}^{\Omega} = 10^{L_{jk}^{\Omega}[\text{dB}]/10}$.

B. HAPS-NIB Backhaul

The BL also undergoes both small-scale fading $\tilde{g}_j$ and large-scale fading L_j^{HAPS} [2]. Hence, the channel coefficient g_j can be expressed as follows:

$$|g_j|^2 = \frac{|\tilde{g}_j|^2 G_j^{\text{HAPS}}}{L_j^{\text{HAPS}}}, \quad (17)$$

where $|\tilde{g}_j|$ is assumed to be Ricean distributed with LOS dominant characteristics between HAPS and UAVB-NIBs. Its probability distribution is given as the magnitude of a circularly-symmetric non-central bivariate normal random variable such as [33]–[35]

$$f(x \mid \nu, \sigma_{\text{f}}) = \frac{x}{\sigma_{\text{f}}^2}\exp\left(\frac{-(x^2+\nu^2)}{2\sigma_{\text{f}}^2}\right) I_0\left(\frac{x\nu}{\sigma_{\text{f}}^2}\right), \quad (18)$$

where I_0 denotes the zeroth-order modified Bessel function of the first kind whose shape parameter K_s is defined by the ratio between the average power of LOS component and the average power associated with NLOS multipath components i.e., $K_s = \nu^2/2\sigma_{\text{f}}^2$. The transmitter antenna gain G_j^{HAPS} from HAPS to the j^{th} UAVB-NIB depends on the antenna aperture efficiency ξ , half-power beamwidth of the antenna $\theta_{\text{HAPS}}^{3\text{dB}}$, HAPS altitude H, UAV altitude H_j and the distance of the UAVB-NIB j from the center of the HAPS beam $\mathbf{c}_0$ with [36]

$$\left[G_j^{\text{HAPS}}\right]_{\text{dB}} = \left[G_0^{\text{HAPS}}\right]_{\text{dB}} - 12\frac{G_0^{\text{HAPS}}}{\xi}\left(\frac{\psi_j}{70\pi}\right)^2, \quad (19)$$

where the peak HAPS antenna beam gain is $G_0^{\text{HAPS}} = \xi\left(70\pi/\theta_{\text{HAPS}}^{3\text{dB}}\right)^2$ and the beam angle (angle of departure) of the j^{th} UAVB-NIB can be derived using

$$\psi_j = \tan^{-1}\left(\frac{\|\mathbf{c}_j - \mathbf{c}_0\|}{H - H_j}\right). \quad (20)$$

Evidently, the antenna directivity gain reduces while moving away from the boresight position in a horizontal plane. Finally, the L_j^{HAPS} is the FSPL as a function of the distance between HAPS and j^{th} UAVB-NIB i.e., d_l^m. We employ the space communication model for the aerial HAPS to compute the received signal path loss L_j^{HAPS} as [37]

$$L_j^{\text{HAPS}} = \frac{16\pi^2 d_j^2}{\lambda^2}, \quad (21)$$

where λ is the wavelength corresponding to the carrier frequency of HAPS. The FSPL renders the ratio between transmit power and received power.

IV. Performance Measure

The overall performance of the system depends on the capacity of the AL as well as the BL. We can evaluate the system performance in terms of achievable sum rate in the access and BL.

We adopt a system where UAVB-NIB serves all RAT Ω users in its coverage area simultaneously. They all share the same bandwidth B_j^{Ω} and transmit with different power and precoding vectors to employ RZF precoding at the receiver for error-free detection. Considering linear precoding, the information rate for user u_{kj}^{Ω} is given by

$$R_{kj}^{\Omega} = B_j^{\Omega}\log_2(1 + \gamma_{kj}^{\Omega}). \quad (22)$$

Consequently, the sum rate of the AL is given by $R_a = \sum_{j=1}^{J}\sum_{k=1}^{K}\sum_{\Omega} R_{kj}^{\Omega}$ which aggregates the downlink data rate from all the UAVB-NIBs to the associated users operating at the desired RAT technologies. Thus,

$$R_a = \sum_{j=1}^{J}\sum_{\Omega} B_j^{\Omega}\sum_{k=1}^{K}\log_2(1 + \gamma_{kj}^{\Omega}). \quad (23)$$

On the other hand, the BL employs DL-NOMA at the HAPS and each UAVB-NIB receives the superposed signal and performs SIC based on the channel strength ordering to decode its own signal. Assuming perfect receiver channel state information (CSI), we get accurate NIB-ordering and error-free decoding. Thus, the achievable rate of j^{th} UAVB-NIB is given by

$$R_j = B_H\log_2\left[1 + \Gamma_j\right]. \quad (24)$$

conditioned on $R_{j\to l} > \tilde{R}_j \;\forall\; j \le l$, where $\tilde{R}_j$ is the target data rate of the j^{th} NIB while $R_{j\to l}$ denotes the rate of the l^{th} NIB to detect j^{th} NIB's message when $j \le l$ in NIB ordering i.e.,

$$R_{j\to l} = B_H\log_2\left(1 + \frac{|g_l|^2 f_j P_H}{|g_l|^2 P_H\sum_{i=j+1}^{J} f_i + \sigma_j^2}\right) \ge \tilde{R}_j. \quad (25)$$

Thus, the sum rate R_b of all UAVB-NIBs can be written as $R_b = \sum_{j=1}^{J} R_j$ yielding

$$R_b = \sum_{j=1}^{J} R_j = B_H\sum_{j=1}^{J}\log_2\left[1 + \Gamma_j\right], \quad (26)$$

where the received SINR at j^{th} NIB in (7) can be expressed using (17) as

$$\Gamma_j = \frac{f_j}{\sum_{i=j+1}^{J} f_i + \aleph_j}, \quad (27)$$

[2]Note that the HAPS station-keeping flight does not contribute to the fast fading since there is no moving scatter surrounding the aircraft [32].

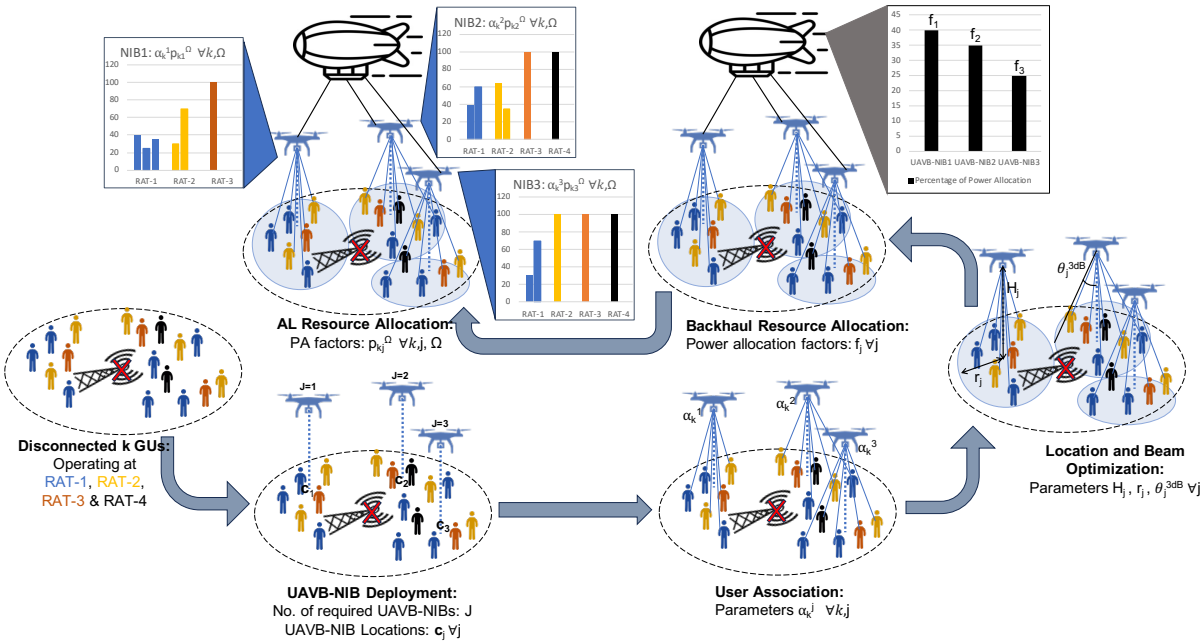

Fig. 3: Schematic Diagram

where,

$$\aleph_j = \frac{\sigma_j^2 L_j^{\text{HAPS}}}{P_H |\tilde{g}_j|^2 G_j^{\text{HAPS}}}. \tag{28}$$

Likewise, the SINR of UAVB-NIB with the strongest channel gain Γ_J in (8) can be manifested using (17) as

$$\Gamma_J = f_J/\aleph_J. \tag{29}$$

V. Problem Formulation and Solution

This work aims to jointly optimize the NIB deployment and resource allocation problems. The deployment challenges include 1) NIB transportation to provide on-demand coverage e.g., backpack NIB, vehicle carrying NIBs, or UAVB-NIB. 2) Number of UAVB-NIBs required to serve a coverage area with a particular set of users and respective user demands (radio access technologies) 3) Optimal deploying locations e.g., 2D locations and altitudes for each participating UAVB-NIB 4) Optimum beam coverage area (dictated by beam radii and beamwidth) to serve the users associated with a given UAVB-NIB. Moreover, the resource allocation problem intends to maximize the sum rate of all users in the coverage area of HAPS while guaranteeing their quality-of-service (QoS), fairness, and expenses within the available power budget. Thus, the optimization problem is targeted at optimizing:

1) UAV deployment: J the number of UAVB-NIB to serve all users in the coverage area, the UAV locations $\mathbf{c}_j$ (i.e., ground projection or center of coverage cells in 2D horizontal plane) and favorable hovering altitudes H_j of each UAVB-NIB.
2) UA: α_k^j the association variable between the users and the UAVB-NIBs for the given β_k^{Ω} i.e., the user demand for particular RAT Ω.
3) Beam optimization signifying the 3dB half-power beam-widths (HPBWs) $\theta_j^{3\text{dB}}$ and beam-radii r_j of each participating UAVB-NIB.
4) NOMA power allocation factors f_j for each UAVB-NIB.
5) NIB power allocation factors p_{kj}^{Ω} for each user in its coverage area demanding a particular RAT service.

A schematic diagram showing the optimization procedures and relevant parameters is given in Fig.3. We formulate the design problem to maximize the sum data rate of all users in the access downlink communication in the heterogeneous communication system as:

$$\mathbf{P1}: \underset{\substack{J,\mathbf{c}_j,H_j,p_{kj}^{\Omega},f_j,\\ \theta_j^{3\text{dB}},r_j,\alpha_k^j \forall k,j}}{\text{maximize}} \sum_{j=1}^{J}\sum_{k=1}^{K}\sum_{\Omega} B_j^{\Omega}\log_2(1+\gamma_{kj}^{\Omega}) \tag{30a}$$

$$\text{s.t.} \quad R_a(\gamma_{kj}^{\Omega}) \le R_b(\Gamma_j),\ \forall\, k \in K_1, j, \Omega \tag{30b}$$

$$R_{kj}^{\Omega} \ge R_{\min}, \quad \forall k,j,\Omega \tag{30c}$$

$$\alpha_k^j \in \{0,1\} \& \sum_{j=1}^{J}\alpha_k^j = 1, \quad \forall k,j \tag{30d}$$

$$\sum_{j=1}^{J}\alpha_k^j \|\mathbf{u}_k - \mathbf{c}_j\| \le \sum_{j=1}^{J}\alpha_k^j r_j, \forall k \tag{30e}$$

$$\theta_{\min} \le \theta_j^{3\text{dB}} \le \theta_{\max}, \forall j \tag{30f}$$

$$H_{\min} \le H_j \le H_{\max}, \forall j \tag{30g}$$

$$R \ge r_j \ge 0.443\lambda^{\Omega} H_j/D, \forall j \tag{30h}$$

$$R_{j\to l} \ge \tilde{R}_j,\ \forall j \le l \tag{30i}$$

$$\sum\nolimits_k \sum\nolimits_{\Omega} \alpha_k^j \beta_k^{\Omega} p_{kj}^{\Omega} \le 1, \quad \forall j \tag{30j}$$

$$0 \le p_{kj}^{\Omega} \le 1, \quad \forall k,j,\Omega \tag{30k}$$

$$\sum\nolimits_j f_j \le 1, \quad \forall j \tag{30l}$$

$$0 \le f_j \le 1, \quad \forall j \tag{30m}$$

$$f_1 \ge f_2 \ge \ldots \ge f_J \tag{30n}$$

$$1 \le J \le K \tag{30o}$$

The constraint (30b) ensures that the sum rate of the GUs in the AL does not exceed the sum rate of the serving UAVB-

NIBs in the BL. The user set K_1 comprises of all users communicating in Scenarios III and IV in Fig. 2. The QoS rate constraint (30c) ensures that each GU is guaranteed the minimum rate threshold $R_{\min}$. The constraint (30d) restricts the Boolean entries $\alpha_k^j \in \{0,1\}, \forall k,j$ (where $1 \leq k \leq K$ and $1 \leq j \leq J$) and the UA limits users to connect to any one UAVB-NIB at a given time for UF and effective utilization of the given resources. Moreover, the constraint (30e) ensures that the associating user resides within the beam coverage area of UAVB-NIB. The essential bounds on the 3dB HPBW, UAVB-NIB altitude, and beam radii, are guaranteed by the constraints (30f), (30g) and (30h), respectively. The spot beams of UAVB-NIB can be adjusted by the beamwidth control. It is worth noting that a narrower beam than the given bounds is not achievable with the given antenna array dimensions. In addition, the rate constraint (30i) warrants the successful information decoding of all NIBs with weaker channel gains at NIBs with strong channel conditions to avoid error propagation. Next, the constraints (30j) and (30k) limit the total transmission power and individual power factor of each GU within the available power budget. The sum of power coefficients of all users operating at Ω within the same NIB coverage cannot exceed 1. Likewise, the power limitations on NIB are given by (30l) and (30m). The optimal NIB power factor ordering in (30n) allocates more power to the weak users and vice versa for UF. Lastly, the bounds on the number of deployed UAVB-NIB are constrained (30o). The optimization problem $\mathbf{P1}$ is a joint deployment and resource allocation problem. The objective function in (30a) and rate constraints in (30b), (30c) are non-convex in terms of optimization variables. Also, constraints (30e) and (30j) contain the products of the optimization variables, and the constraint in (30d) renders **P1** as a non-convex mixed-integer programming (MIP) problem. It is NP-hard, meaning that in general we don't have a polynomial-time algorithm to solve it [38]. Therefore, we will divide this problem into sub-problems and solve these sub-problems sequentially and iteratively using the alternate optimization to find a feasible solution.

Next, we present the sub-problems and how each of them can be solved for fewer optimization parameters assuming that other design parameters are fixed.

A. UAVB-NIB Deployment

The deployment problem requires the identification of the number of UAVB-NIBs J and their respective locations $\mathbf{c_j}\forall\mathbf{j}$ to cover a remote area of radius R and user distribution K. Each NIB hovering at an altitude H_j offers the coverage to the ground circular area using high-density narrow spot beam with beamwidth $\theta_j^{3\text{dB}} \in \mathbb{R}$, beam radius $r_j \in \mathbb{R}^+$, and beam location[3] $\mathbf{c}_j \in \mathbb{R}^2$ for all $j \in \{1,2,\ldots,J\}$ as detailed in Fig. 2. The variable J ranges between $1 \leq J \leq K$, meaning that there must be at least one NIB to serve all GUs or a maximum of K UAVB-NIBs to individually serve each user. The lower bound of 1 is unrealistic for a large coverage area as the UAVB-NIB has a limited coverage whereas the upper bound of K is economically unsuitable. A large fleet of UAVB-NIBs can effectively improve the system performance but it is not resource-efficient. In essence, the value of J is a trade-off between SINR and efficient allocation of given resources. A larger J renders highly directional beams with concentrated power, improved SINR, and consequently higher data rates but inefficient use of UAVB-NIBs. Therefore, the deployment problem is converted to the minimization problem which evaluates the minimum number of UAVB-NIBs and their respective locations to cover the given set of ground users. The UAVB-NIB altitude and coverage radius are related to each other through half-power beamwidth of the spot beam as:

$$r_j = H_j \tan\left(\frac{\theta_j^{3\text{dB}}}{2}\right). \tag{31}$$

Intuitively, for a given HPBW of NIB antennas, we can increase or decrease the UAV altitude to adjust the beam radius for suitable coverage. Our findings reveal that R_a monotonically increases with J, but it is not economically feasible to deploy such a large number of UAVB-NIBs. The problem can have multiple solutions based on the economic constraints:

- Based on the relation $r_j = H_j \tan\theta_j$, we can use the lower bounds of the UAVB-NIB altitude and beam width to find the minimal possible beam radius.
- Find $r_j \forall j$ which satisfies the constrained inequality (30b) with equality i.e., $R_a = R_b$.

Problem **P1** can be decomposed as the sub-problem **P1(a)** for optimal UAVB-NIBs deployment given the beam coverage radius $r_j \forall j$;

$$\textbf{P1(a)}: \underset{J,\mathbf{c}_j}{\text{minimize}}\ J \tag{32a}$$

$$\text{s.t.} \quad (30\text{d}), (30\text{e}), (30\text{o}) \tag{32b}$$

This sub-problem finds the optimal locations (beam centers w_m) of the minimal number of beams required to cover the users in the disk of radius R i.e., the coverage area of HAPS communication system. Problem **P1(a)** is a well-known geometric disk cover (GDC) problem which aims to find minimum number of disks of given radius to cover a set of points in the plane. The famous GDC problem is NP-hard highlighting the NP-hardness of **P1(a)**.

The problem can alternately be reformulated as the identification problem for a set of points:

$$\textbf{P1(a1)}: \underset{\mathbf{z}\in\mathbb{B}^K}{\text{minimize}} \mathbf{1}^{\mathrm{T}}\mathbf{z} \tag{33a}$$

$$\text{s.t.} \quad \mathbf{z}_k \in \{0,1\}, \forall k \tag{33b}$$

$$\mathbf{D}\mathbf{z} \geq \mathbf{1} \tag{33c}$$

where $\mathbf{D}$ is the symmetric boolean matrix with entries

$$d_{kl} = \begin{cases} 1, & \|\mathbf{u}_k - \mathbf{u}_l\|_2 \leq r_j, \\ 0, & \text{otherwise.} \end{cases} \tag{34}$$

To summarize, this problem identifies the minimum possible set of points from all the user coordinates such that if we draw the circles of radius r_j around these points then it will encompass all the points in it's surrounding. We mark this set of points as the UAVB-NIB central positions and $\sum z^* = J^*$. This is a linear programming problem which can be easily solved using Lagrange function and KKT conditions for lower dimensions. The *intlinprog* package in MATLAB

[3]Beam location indicates the center of the beam with maximum antenna gain in the boresight direction

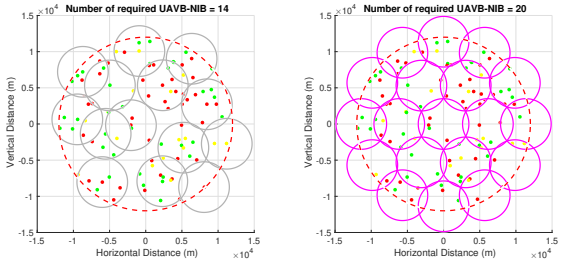

(a) GDC Approach (b) Cellular Approach

Fig. 4: Required number of UAVB-NIBs for user-connectivity in a given coverage area

can efficiently yield the UAVB-NIB deployment parameters for higher dimensional problems. Fig. 4 illustrates an example deployment strategy for the coverage of a given set of users. GDC approach requires 14 UAVB-NIBs in Fig. 4(a) as opposed to 20 required in Fig. 4(b) using conventional cellular approach. Hence, without optimization, the use of 14 NIBs is not enough and will lead to coverage holes or user outage. With optimization, 6 out of the 20 NIBs can be saved, leading to 30% improvement in resource efficiency.

B. Association Parameter

We assume that all NIBs are capable of operating at all RATs depending on the demands from the associated users. In this context, any user can connect to any UAVB-NIB. However, for UF and higher system efficiency, each user is allowed to associate with one and only one UAVB-NIB. Intuitively, the sum rate is maximized when the SINR γ_{kj}^{Ω} is maximized (for a given bandwidth for Ω RAT) owing to the monotonically increasing nature of logarithmic functions for $\gamma_{kj}^{\Omega} > 0$. Hence, the UA problem aims at finding the association parameters $\alpha_k^j,\ \forall k, j$ can be restructured as subproblem **P1(b)**:

$$\textbf{P1(b)}: \underset{\alpha_k^j,\ \forall k,j}{\text{maximize}} \sum_{j=1}^{J}\sum_{k=1}^{K}\sum_{\Omega}\gamma_{kj}^{\Omega}\left(\alpha_{kj}^{\Omega}\right) \tag{35a}$$

$$\text{s.t.} \qquad \text{(30d) and (30e).} \tag{35b}$$

Constraint (30e) ensures that all the associated users of UAVB-NIB reside within its coverage area inside the main lobe of the antenna beam to be served simultaneously [39]. However, it is noteworthy that a user k may reside within the radius of UAVB-NIB j while being associated with another UAVB-NIB j' in overlapping coverage zones. The solution to this association parameter problem can be quantified using the greedy algorithm as:

$$\alpha_k^j = \begin{cases} 1, & \gamma_k^j \geq \gamma_k^{j'}\ \forall j' \in \{1,2,\ldots,J\}\backslash j \\ 0, & \text{otherwise.} \end{cases} \tag{36}$$

In practice, all the deployed UAVB-NIBs broadcast paging signals and the users can associate and connect to the one with the maximum received signal power [40].

C. Location Optimization

Consider the perfect CSI and RZF precoding to nullify co-channel interference between the users and decouple their information bearing signals. The UAVB-NIB localization problem is aimed at improving the channel gain between the UAVB-NIB and the associated users which will resultantly increase the SINR and AL rates in downlink communication scenario. The channel gain can be improved by adjusting the UAVB-NIB location parameters to enhance the scaling factors in (10) i.e., maximizing the antenna beam gain and minimizing FSPL. The higher antenna beam gain can be attained by using highly directional beams with concentrated radio frequency power, whereas, the FSPL can be decreased by adjusting UAVB-NIB altitude. Based on the derived J and α_k^j for a given beam coverage radius $r_j\ \forall j$, we now carry out the location parameter optimization i.e., $\mathbf{c}_j, r_j, H_j, \theta_j^{3\text{dB}}$,and $\phi_j^{3\text{dB}}$ for the worst-case scenario i.e., maximizing the minimum channel gain and minimizing the maximum path loss. Interestingly, these variable are related rendering only three independent variables $\mathbf{c}_j, r_j, \phi_j^{3\text{dB}}$ while other location parameters can be derived from these independent parameters using $\theta_j^{3\text{dB}} = \pi/2 - \phi_j^{3\text{dB}}$ and $H_j = r_j \tan(\phi_j^{3\text{dB}})$.

$$\textbf{P1(c)}: \underset{\mathbf{c}_j, r_j, {\phi_j}^{3\text{dB}}}{\text{maximize}}\ \min_{k,\Omega}\ \alpha_k^j(G_{jk}^{\Omega}[\text{dB}] - L_{jk}^{\Omega}[\text{dB}]) \tag{37a}$$

$$\text{s.t.} \qquad r_j \geq \max\{\alpha_k^j \|\mathbf{u}_k - \mathbf{c}_j\|\}, \forall k, j \tag{37b}$$

$$\text{(30f), (30g), (30h), and (31)} \tag{37c}$$

The sub-problem **P1(c)** is disjoint problem for all j UAVB-NIBs and hence it can be solved independently for all UAVB-NIBs with the given set of associated users. The joint optimization of **P1(c1)** is difficult and complex owing to the non-convex nature due to the mixture of bessel functions, exponential functions, sinusoidal functions and multiple optimization parameters. Thus, it is hard to achieve a global optimal solution. However, decomposing this problem into sub-problems is a promising choice to obtain sub-optimal solution close to the optimal one. We can then employ block coordinate descent (BCD) method for alternate optimization of the parameters to successively maximize the objective functions along one coordinate while fixing the local values at the other coordinates in each iteration. This method guarantees local stationary point because objective function is monotonically increasing in each coordinate with every iteration i.e., $f(\mathbf{c}_j, r_j, {\phi_j}^{3\text{dB}}) \leq \max f(\mathbf{c}_j, r_j | {\phi_j}^{3\text{dB}}) \leq f(\mathbf{c}_j^*, r_j^*, {\phi_j}^{3\text{dB}}) \leq \max f({\phi_j}^{3\text{dB}} | \mathbf{c}_j^*, r_j^*) \leq f(\mathbf{c}_j^*, r_j^*, {\phi_j}^{3\text{dB}*})$.

Considering the objective function $f(\mathbf{c}_j, r_j | {\phi_j}^{3\text{dB}})$ for j^{th} UAVB-NIB, the problem is equivalent to the minimum enclosing circle problem for a given set of points (users associated with j^{th} UAVB-NIB). Maximum sum rate can be achieved with maximum SNR by choosing minimum possible r_j to enclose all the points in a circle centered at $\mathbf{c}_j$. This will ensure highly directional beam and concentrated power to serve the given set of users. This can be reformulated as a quadratic programming problem in **P1(c1)**

$$\textbf{P1(c1)}: \underset{\kappa \in \mathbb{R}^{\varsigma_j}}{\text{minimize}}\ \kappa^{\text{T}} \boldsymbol{\Xi}_j \kappa - \mathbf{d}_j^{\text{T}} \kappa \tag{38a}$$

$$\text{s.t.} \qquad \sum_{n=1}^{\varsigma_j} \kappa_n = 1, \quad \kappa_n \geq 0 \quad \forall n \tag{38b}$$

where $\boldsymbol{\Xi}_j = \mathbf{U}_j \mathbf{U}_j^{\text{T}}$ and $\mathbf{d}_j = \text{diag}(\boldsymbol{\Xi}_j)$ with

$$\mathbf{U} = [\mathbf{u}_1; \mathbf{u}_2; \ldots; \mathbf{u}_K] \in \mathbb{R}^{K \text{x} 2},$$

$$\mathbf{U}_j \in \mathbb{R}^{\varsigma_j \text{x} 2}, \mathbf{U}_j \subseteq \mathbf{U}, \{\mathbf{u}_k \in \mathbf{U}_j | \alpha_k^j = 1\}.$$

Moreover, $\varsigma_j = \sum_{k=1}^{K} \alpha_k^j$ is the number of users associated

with j^{th} UAVB-NIB. The Lagrange function of the revised problem **P1(c1)** can be written as:

$$\mathcal{L}(\iota,\kappa) = \kappa^{\mathrm{T}}\boldsymbol{\Xi}_j\kappa - \mathbf{d}_j^{\mathrm{T}}\kappa - \iota(\sum_{n=1}^{\varsigma_j}\kappa_n = 1); \iota \geq 0. \tag{39}$$

Solving this convex dual problem renders the primal and dual variables, which can then yield $\mathbf{c}_j^* = \mathbf{U}_j^{\mathrm{T}}\kappa^*$ and $r_j^* = \sqrt{\kappa^{*\mathrm{T}}\boldsymbol{\Xi}_j\kappa^* - \iota^*}$. Based on the UAVB-NIB horizontal locations, we can now adjust individual altitudes using the optimal elevation angles $\phi_j^*\ \forall j$, by solving the following (see Appendix A) [41]

$$\frac{A}{1+\bar{a}e^{-b\phi_{jk}^{\Omega}}} + 20\log_{10}(r_j\sec\phi_{jk}^{\Omega}) + \bar{B}^{\Omega} = 0, \tag{40}$$

where $\bar{a} = ae^{ab}$. Interestingly, the evaluation of the optimal HPBW $\theta_j^{*3\mathrm{dB}}$ and altitude H_j^* for each participating UAVB-NIB is a disjoint problem and can be solved independently.

D. Resource Allocation

After UAV deployment, UA, and beam optimization, we focus on the design of power allocation parameters for the BL. HAPS employs downlink NOMA strategy to simultaneously serve all the NIBs in its coverage area based on their locations and channel strength ordering. Thus, the power allocation problem for HAPS-NIB BL can be written as:

$$\textbf{P1(d)}: \underset{\boldsymbol{f_j}}{\text{maximize}} \sum_{j=1}^{J} R_j\left(\Gamma_j\right) \tag{41a}$$

$$\text{s.t.} \quad R_{j\to l} \geq \tilde{R}_j,\ \forall j \leq l \tag{41b}$$

$$\sum\nolimits_j f_j \leq 1, \quad \forall j \tag{41c}$$

$$0 \leq f_j \leq 1, \quad \forall j \tag{41d}$$

$$f_1 \geq f_2 \geq \ldots \geq f_J \tag{41e}$$

Given the UAVB-NIB ordering $N_1 \leq N_2 \leq \ldots \leq N_J$ with respect to their channel strengths, the target threshold constraint $R_{j\to l} \geq \tilde{R}_j,\ \forall j \leq l$ is most difficult to meet in the worst case scenario i.e., $j = l$. Thus, focusing on the worst case scenario, the constraint (41b) can simplified as $R_j \geq \tilde{R}_j,\ \forall j$. Moreover, considering the same target threshold for all NIBs i.e., $\tilde{R}_j = R_{\text{th}}$, we can present the closed-form solution to this problem as [42]:

For the given UAVB-NIBs, there exists a UAVB-NIB $\jmath$ in $1 \leq \jmath \leq J$, which satisfies the following condition:

$$\begin{cases} \left(2^{R_{\text{th}}/B_H} - 1\right)\left(\sum\limits_{i=\jmath}^{J} \aleph_i 2^{(i-1)R_{\text{th}}/B_H}\right) \leq 1, \\ \left(2^{R_{\text{th}}/B_H} - 1\right)\left(\sum\limits_{i=\jmath-1}^{J} \aleph_i 2^{(i-1)R_{\text{th}}/B_H}\right) \geq 1. \end{cases} \tag{42}$$

which indicates that the NIBs $\jmath$ to J can achieve the target rate threshold R_{th} owing to the better channel conditions, whereas, the NIB $\jmath-1$ and weaker NIBs are unable to achieve the minimum threshold with the given power budget. Thus, we allocate the remaining power to the strongest NIB in order to maximize the sum data rate. Hence, the maximum achievable sum rate R_b^*, the power coefficients of NIBs f_j and the remaining power fraction Δf are given by

$$R_b^* = (J-\jmath)\,R_{\text{th}} + B_H\log_2\left[1 + \frac{\Delta f}{1-\Delta f+\aleph_J}\right], \tag{43}$$

Algorithm 1 Sequential Optimization Algorithm

Input: The number $\{K\}$, the coordinates of users $\{\mathbf{u}_k\}$ in the horizontal plane, radius of desired coverage area $\{R\}$, UAVB-NIB operable RATs Ω, users RAT preference β_k^{Ω}, NIB transmission power for each RAT $P_j^{\Omega}\ \forall\Omega$, HAPS transmission power P_H, UAVB-NIBs transmission power P_j^{Ω} and station-keeping altitude $\{H\}$.
Initialize $i \leftarrow 0$, $R_a[i-1] \leftarrow R_0$ and $\epsilon \leftarrow \infty$
Select QoS minimum rate threshold $R_{\min}$, minimum possible beam radius $r_{\min}$, and regularization scalar ω
Set tolerance δ, $r[i] = r_{\min}$, and $r_{\text{UB}} = R$
Choose Δr and identical beam radius $r_j[i] = r[i]\forall m$
while $\epsilon \geq \delta$ & $r_{\min} \leq r_j[i] \leq R$ **do**
  Let $i \leftarrow i+1$
  Update $r_j[i] = r_j[i-1] + \Delta r$ for all UAVB-NIBs ensuring sequential increment with every iteration.
  Determine $M[i]$ and $\mathbf{c}_j[i]\ \forall\ m \in [1, M]$ using GDC to solve **P1(a1)** in (33) given constant $r[i]$.
  Associate users by solving **P1(b)** in (35) to evaluate $\alpha_k^j[i]$ using greedy algorithm.
  Optimize individual UAVB-NIB to valuate beam parameters $\tilde{w}_j[i]$, $\tilde{\theta}_j[i]$ and $\tilde{r}_j[i]$ by solving **P1(c1)** in (38).
  Update $w_j[i] \leftarrow \tilde{w}_j[i]$, $r_j[i] \leftarrow \tilde{r}_j[i]$ and $\theta_j[i] \leftarrow \tilde{\theta}_j[i]$.
  Obtain the available transmit power $P_H[i]$ of a solar powered HAPS at the chosen location on a given date and time of the day using the power estimation algorithms [29].
  Calculate the channel coefficients $g_j[i]$ and $h_{kj}^{\Omega}[i]$ using the pathlosses $L_j^{\text{HAPS}}[i]$ and beam gain $G_j^{\text{HAPS}}[i]\ \forall j$ for the backhaul and pathloss $L_{jk}^{\Omega}[i]$ and beam gain $G_{jk}^{\Omega}[i]\ \forall j,k,\Omega$ for the AL, respectively.
  Compute the power allocation coefficients $f_j[i]$ for each UAVB-NIB using the closed form solutions of **P1(d)** in (41) for the given QoS threshold $\tilde{R}_j$ and NIB ordering.
  Compute the power allocation coefficients $p_{kj}^{\Omega}[i]$ for each user by solving **P1(e)** in (46).
  Evaluate the sum rate in the AL $R_a[i]$ and backhaul sum rate $R_b[i]$
  Compare $R_a[i]$ with $R_a[i-1]$
  if $R_a[i] \geq R_a[i-1]$: $R_a^*[i] \leftarrow R_a[i]$
  if $R_a[i] \leq R_a[i-1]$: $R_a * [i] \leftarrow R_a[i-1]$
  Update $\epsilon \leftarrow R_a[i] - R_a[i-1]$
end while
User grouping parameters: $J^* \leftarrow J[i]$, $\mathbf{c}_j^* \leftarrow \mathbf{c}_j[i]$
UA parameters: $\alpha_k^{j*} \leftarrow \alpha_k^{j*}[i]\ \forall\ l, m$
Beam radii: $r_j^* \leftarrow r_j[i]$
Half-power beam widths: $\theta_j^* \leftarrow \theta_j[i]\ \forall\ m$
Backhaul power allocation parameters: $f_j^* \leftarrow f_j[i]\ \forall\ j$
AL power allocation parameters: $p_{kj}^{\Omega*} \leftarrow p_{kj}^{\Omega}[i]\ \forall\ k,j,\Omega$
Sum rate of GUs: $R_a^* \leftarrow R_a[i]$

$$\hat{f}_j = \left(2^{R_{\text{th}}/B_H} - 1\right)\left(\sum_{k=j+1}^{J} \hat{f}_k + \aleph_j\right), \tag{44}$$

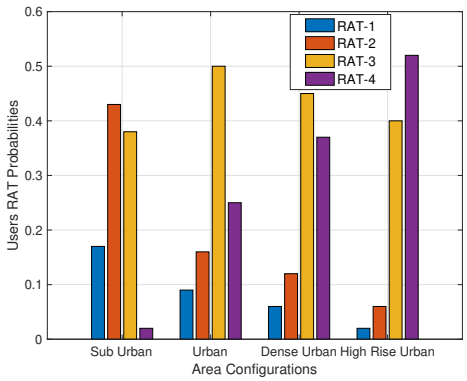

Fig. 5: Users RAT Probabilities (Pr_{Ω})

$$\Delta f = 1 - \left(2^{R_{\mathrm{th}}/B_H} - 1\right)\left(\sum_{i=\jmath}^{J} \aleph_i 2^{(i-1)R_{\mathrm{th}}/B_H}\right). \quad (45)$$

The optimal sum rate in (43) comprises of two terms; the first term is the target rate threshold of NIBs $\jmath$ to J, whereas the second term is the additional rate of NIB J using the leftover power Δf. This indicates that NIBs $\jmath$ to J can attain target rates with assigned power coefficients $\hat{f}_{\jmath}$, $\hat{f}_{\jmath+1}$,..., $\hat{f}_J$ using (44). The remaining power with power allocation coefficient Δf is insufficient for any of the remaining NIBs 1 to $\jmath-1$ to fulfill their target threshold rate. Therefore, Δf in (45) is assigned to the strongest NIB J in order to maximize the overall sum rate.

Next is the resource allocation for the AL. The sum rate of the AL in scenarios III and IV is upper bounded by the rate of the BL (43) derived by solving problem **P1(d)**. This subproblem is enumerated in problem **P1(e)**:

$$\textbf{P1(e)}: \underset{p^{\Omega}_{kj}\forall k}{\text{maximize}} \sum_{j=1}^{J}\sum_{k=1}^{K}\sum_{\Omega} B^{\Omega}_{j}\log_2(1+\gamma^{\Omega}_{kj}) \quad (46a)$$

$$\text{s.t.} \quad \tilde{R}_a(\gamma^{\Omega}_{kj}) \le R^{*}_{b}, \quad \forall\, k \in K_1, j, \Omega \quad (46b)$$

$$R^{\Omega}_{kj} \ge R_{\min}, \quad \forall\, k, j, \Omega \quad (46c)$$

$$\sum\nolimits_{k}\sum\nolimits_{\Omega} \alpha^{j}_{k}\beta^{\Omega}_{k}p^{\Omega}_{kj} \le 1, \quad \forall j \quad (46d)$$

$$0 \le p^{\Omega}_{kj} \le 1, \quad \forall k, j, \Omega \quad (46e)$$

where $\tilde{R}_a(\gamma^{\Omega}_{kj})$ is the subset of the AL rate comprising of the data rates of the set of users $k \in K_1$ in scenarios III and IV, which utilize the BL for end-to-end communications. Assuming perfect RZF, we get $|\mathbf{h}^{\Omega H}_{kj}\mathbf{w}^{\Omega}_{lj}|^2 = 0,\ \forall k \neq l$. Thus, using (4), the objective function reduces to

$$R_a(p^{\Omega}_{kj}) = \sum_{j=1}^{J}\sum_{k=1}^{K}\sum_{\Omega} B^{\Omega}_{j}\log_2\left(1+\bar{\gamma}^{\Omega}_{kj}|\mathbf{h}^{\Omega H}_{kj}\mathbf{w}^{\Omega}_{kj}|^2\alpha^{j}_{k}\beta^{\Omega}_{k}p^{\Omega}_{kj}\right). \quad (47)$$

The simplified expression shows an ideal concave objective function as the weighted sum of the logarithmic functions and convex constraints without (46b). For this non-convex constraint (46b), we propose to employ successive convex approximation (SCA) and find the convex approximation $\tilde{R}_a$ and solve this problem iteratively. The first-order Taylor series approximation[4] $\tilde{R}_a$ around the power coefficient variables is given by:

$$\tilde{R}_a(\mathbf{p}, \mathbf{p}^{(i)}) \approx \tilde{R}_a(\mathbf{p}^{(i)}) + \nabla_{\mathbf{p}}\tilde{R}_a(\mathbf{p}^{(i)})^{\mathrm{T}}(\mathbf{p}-\mathbf{p}^{(i)}), \quad (49)$$

where, $\mathbf{p}$ is the vector comprising of the power coefficients of all users depending on their UAB-NIB association and demanded RAT and $\mathbf{p}^{(i)}$ is the chosen/updated power coefficients vector at instant (i). The gradient $\nabla_{\mathbf{p}}\tilde{R}_a$ can be evaluated using the following partial derivatives:

$$\nabla_{\mathbf{p}}\tilde{R}_a = \left[\alpha^{j}_{1}\beta^{\Omega}_{1}\frac{\partial\tilde{R}_a}{\partial p^{\Omega}_{1j}} \quad \alpha^{j}_{2}\beta^{\Omega}_{2}\frac{\partial\tilde{R}_a}{\partial p^{\Omega}_{2j}} \quad \dots \quad \alpha^{j}_{K}\beta^{\Omega}_{K}\frac{\partial\tilde{R}_a}{\partial p^{\Omega}_{Kj}}\right], \quad (50)$$

where

$$\frac{\partial\tilde{R}_a}{\partial p^{\Omega}_{kj}} = \sum_{j}\sum_{\tilde{k}}\sum_{\Omega}\frac{B^{\Omega}_{j}}{\log(2)}\frac{\bar{\gamma}^{\Omega}_{kj}|\mathbf{h}^{\Omega H}_{kj}\mathbf{w}^{\Omega}_{kj}|^2\alpha^{j}_{k}\beta^{\Omega}_{k}}{1+\bar{\gamma}^{\Omega}_{kj}|\mathbf{h}^{\Omega H}_{kj}\mathbf{w}^{\Omega}_{kj}|^2\alpha^{j}_{k}\beta^{\Omega}_{k}p^{\Omega}_{kj}}. \quad (51)$$

It is interesting to note that the gradient $\nabla_{p^{\Omega}_{kj}}\tilde{R}_a$ can be conveniently computed owing to the disjoint data rate of each user as a function of the allocated power fraction. This leads to the convex approximation of the constraint (46b). Thus, problem **P1(e)** can be iteratively solved using the successive convex approximation method. The non-convex mixed integer programming problem **P1** can be solved using the convexification of each individual sub-problem. Each sub-problem is then independently solved for fewer variables, assuming the rest as given constants, as detailed in Algorithm 1. Although the sub-problems are solved independently, however, the presented sequential order is crucial. It is pivotal to evaluate the serving number and locations of UAVB-NIB before user association. Deployment enables users to associate with the nearest UAVB-NIB rendering maximum signal strength. Likewise, UA helps in location optimization to form directive beams. Eventually, deployment and association permits the optimal resource allocation from the identified UAVB-NIB to the group of associated users demanding particular RATs.

E. Complexity Analysis

In this subsection, the complexity of each subproblem is analyzed in order to evaluate the overall computational complexity.

P1(a): The classic geometric disk cover is a NP-hard problem with complexity $\mathcal{O}(2^K)$. The equivalent problem **P1(a1)** can be solved by finding the distance matrix and then sorting the points into circles with the given radius, which has the complexity $\mathcal{O}(K\log K)$.

P1(b): The greedy algorithm for the user association problem associates K users to one of the J UAVB-NIBs having maximum SNR, with complexity $\mathcal{O}(KJ)$.

P1(c): The location optimization sub-problem can be effectively treated as a minimum enclosing circle problem with complexity ranging from linear to quadratic. The proposed solution (39) has linear complexity for each enclosing circle i.e., $J\mathcal{O}(K) = \mathcal{O}(JK)$. On the other hand, using the Newton-Raphson method to solve (40) has a complexity of $\mathcal{O}(J)$. The

[4]s First order Taylor series expansion of a function $f(x)$ around a point $x^{(k)}$ is given as

$$\tilde{f}\left(x, x^{(k)}\right) \approx f\left(x^{(k)}\right) + \nabla_x f\left(x^{(k)}\right)\left(x - x^{(k)}\right). \quad (48)$$

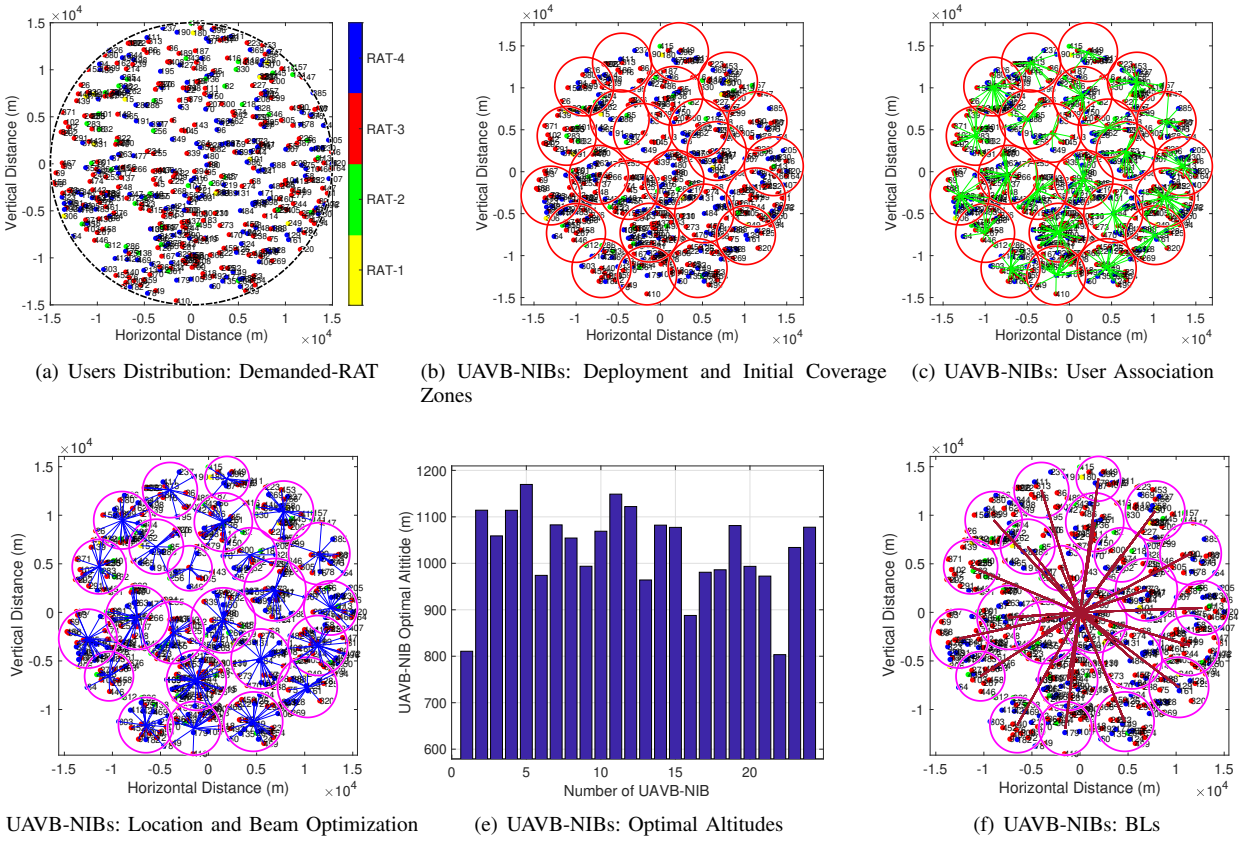

(a) Users Distribution: Demanded-RAT (b) UAVB-NIBs: Deployment and Initial Coverage Zones (c) UAVB-NIBs: User Association

(d) UAVB-NIBs: Location and Beam Optimization (e) UAVB-NIBs: Optimal Altitudes (f) UAVB-NIBs: BLs

Fig. 6: UAVB-NIBs deployment, user association and parameters optimization

accumulative complexity of the BCD algorithm with I_{BCD} iterations (until convergence) is $\mathcal{O}(I_{\mathrm{BCD}}J(K+1))$.

P1(d): The proposed NOMA power allocation subproblem can be solved with complexity $\mathcal{O}(JK\log K)$.

P1(e): The resource allocation employs SCA to iteratively solve the convex sub-problem. Each sub-problem can be used using the interior-point method with complexity $\mathcal{O}(K^3)$. For I_j iterations to converge to the desired results, the computational complexity for J UAVB-NIBs is $\prod_{j=1}^{J}\mathcal{O}(I_jK^3)$. If the maximum number of iterations for any one UAVB-NIB is I_{RA}, we can upperbound the complexity of sub-problem $\mathbf{P1}(\mathbf{e})$ as $\mathcal{O}(JI_{\mathrm{RA}}K^3)$.

The overall complexity of the proposed Algorithm 1 is:

$$\mathfrak{C}=\mathcal{O}(I_{\mathrm{AO}}(KJ+I_{\mathrm{BCD}}J(K+1)+(1+J)K\log K+I_{\mathrm{RA}}JK^3)), \tag{52}$$

where I_{AO} is the number of iterations of the alternate optimization algorithm until convergence. Thus, the overall computational complexity is dominated by the resource allocation problem $\mathbf{P1}(\mathbf{e})$. In this case, the complexity $\mathfrak{C}$ can be simplified as $\mathfrak{C}=\mathcal{O}(I_{\mathrm{AO}}I_{\mathrm{RA}}JK^3)$.

VI. Numerical Results and Discussion

We adopt PHASA-35 HAPS aircraft model flying at an altitude of 20km and evaluate the available transmit power for noon on the winter and summer solstice of 2025 using the solar algorithms [29]. The analysis assumes different areas: sub urban, urban, dense urban, and high rise urban with different user densities, where users follow a Poisson point process. In addition, each UAVB-NIB is capable of offering 4 RAT technologies to the GUs with different probabilities according to the user population, as illustrated in Fig. 5. If any specific RAT is not available on a particular UAVB-NIB, those users requesting this RAT will be disconnected by the NIB. We assume distinct carrier frequencies and appropriate bandwidths for each RAT technology. We aim to carry out a thorough numerical analysis to quantify the gains achieved by each step in the proposed heterogeneous communication system.

A. Illustration of the Proposed Sequential Algorithm

The sequential optimization of the proposed UAVB-NIB deployment, UA, and location optimization is illustrated in Fig. 6. Color-coded users operating at different RATs and distributed as Poisson point process in the circular HAPS coverage area of 150km radius are demonstrated in Fig. 6(a).RAT-1(yellow) is the least probable whereas RAT-4(blue) is the preferred access technology for the GUs in this configuration area using the probabilities in Fig. 5. Next, we determine the initial coverage zones for UAVB-NIB deployment using the GDC algorithm, which render 24 required UAVB-NIBs and their central locations for a given beam radius as depicted in Fig. 6(b). It is followed by the UA using greedy algorithm where the users associate themselves with the UAVB-NIB based on the maximum received SINR. Fig. 6(c) presents the UA using green lines merging towards the beam center marked by the UAVB-NIB's projection on ground. This UA allows us to concentrate the antenna beams towards the active users

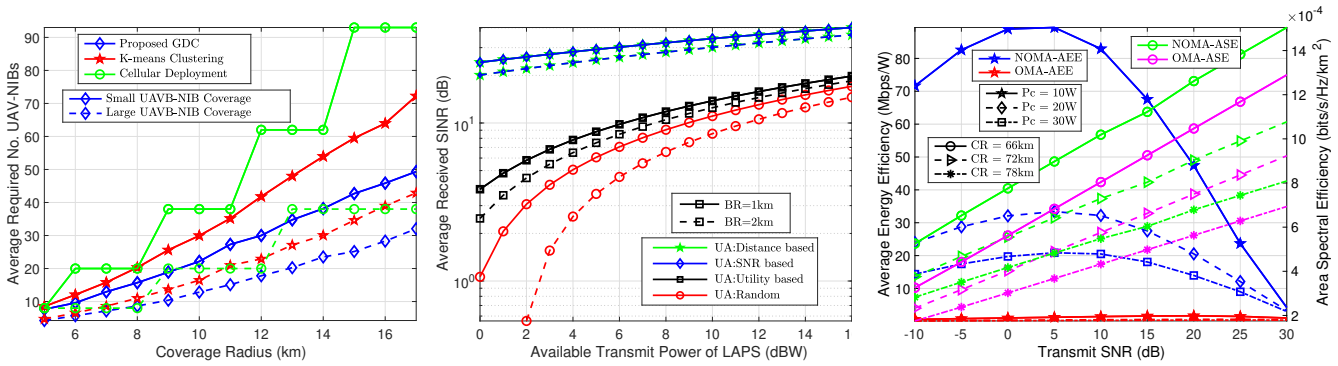

(a) Proposed UAVB-NIB Deployment (b) Different user association schemes (c) AEE and ASE of Backhaul

Fig. 7: Parameters optimization and resource allocation

while optimizing the beams parameters and UAVB-NIBs locations. Fig. 6(d) exhibits the optimal UAVB-NIB locations and reduced coverage/beam radii to serve the predefined associated users. Clearly, this minimizes the overlapping regions and maximizes the power density in a given beam which increases the SINR and consequently the sum-rate of the users. On the other hand, optimal flying altitudes of the 24 participating UAVB-NIBs are highlighted in Fig. 6(e). Eventually, Fig. 6(f) displays the backhaul connection of each UAVB-NIB with the HAPS positioned at the origin without loss of generality. Fig. 6 displays the step-by-step approach to tackle the UAVB-NIB deployment and UA problems. These optimized parameters can then be utilized for optimal resource allocation by UAVB-NIBs and HAPS in the access and backhaul downlink, respectively.

B. UAVB-NIB Deployment Schemes

In order to validate the effectiveness of UAVB-NIB deployment algorithm, we study the minimum number of required UAVB-NIBs in a sub-urban area with user density 1000 users/km^2 and radius ranging from 5km to 17km. We assume two different coverage capabilities of the participating UAVB-NIBs termed as small and large UAVB-NIB coverage with beam radii 2.5km and 3.5km, respectively. Evidently, the number of required UAVB-NIBs increases with the increasing coverage radius and consequently increasing number of GUs in that area as detailed in Fig. 7(a). Intuitively, a large number of narrow-beamed UAVB-NIBs are required to serve a certain coverage area as compared to the wide-beamed UAVB-NIBs. We compare the proposed solution of GDC problem with the state-of-the-art k-means clustering algorithm and the conventional cellular deployment. In the cases considered, the proposed GDC scheme renders significantly less number of required UAVB-NIBs than the conventional methods to provide coverage for the same GUs. The step-wise increase in the conventional cellular deployment is owing to the increase in the tier of UAVs for a certain change in coverage radius which then stays the same for a range of coverage radii before adding another tier/layer of UAVs. The proportional relationship between the coverage radius and the corresponding required number of UAVB-NIBs is evident in Fig. 7(a). For a given beam radius, the scarcity of UAVB-NIBs can only cover a small coverage area. For a coverage radius of around 16km, the proposed GDC demands 45 narrow-beamed UAVB-NIBs, which is 64 for the k-means clustering algorithm and 93 for the cellular approach. Likewise, the proposed GDC renders 23 wide-beamed UAVB-NIBs, which is 30 for the k-means clustering and 38 for cellular approach to serve 14km coverage area. We can conclude that the proposed deployment scheme can serve a given coverage area with significantly less UAVB-NIBs than the k-means or conventional deployment.

C. Performance of Different UA Strategies

We compare the performance of the proposed SNR-based UA (UA-SNR) algorithm with the distance-based UA association (UA-DB), the random association UA (UA-Rand), and a popular utility-based association (UA-Utility) in Fig. 7(b). The utility-based algorithm associates the users with the UAVB-NIBs using a utility function which not only incorporates the received signal strengths but also incorporates the load balancing amongst various UAVB-NIBs. We investigate the average received SINR at the GUs in the same sub-urban setting with narrow-beamed and wide-beamed UAVB-NIBs. For a given user distribution, we evaluate the optimal number and locations of the UAVB-NIBs. Then, we perform user-association with pre-defined UAVB-NIBs locations using the four aforementioned UA algorithms to study the average received SINR of the GUs. Expectedly, the average received SINR increases with the increased transmission power and especially for the narrow-beamed UAVB-NIBs. We notice the percentage reduction of upto 80.76% in average received SINR when the UAVB-NIB transmit power is reduced from 16dBW to 0dBW while employing UA-Utility. Interestingly, the UA-DB performs equally well as the proposed UA-SNR but better than UA-Utility, whereas UA-Rand demonstrates degraded performance for the entire range of transmission power. Using 10dBW transmission power for each participating UAVB-NIB, we observe almost 17dB and 21dB difference in the average received SINR of the GUs, signifying the advantage of the proposed UA over the utility-based or random UA.

D. Energy and Spectral Efficiency of the Backhaul

Aerial communications are predominantly restricted by the available power budget [29]. This manifests energy efficiency[5] as a critical performance metric for the solar-powered HAPS. Energy efficient communication with cognizant power control can significantly impact and prolong the flight operation times. We can compute the average energy efficiency (AEE) of the BL $\mathrm{AEE_b}$ using

$$\mathrm{AEE}_b = \frac{1}{J}\sum_{j=1}^{J}\frac{R_j}{f_j P_H + P_{c_2}}, \tag{53}$$

where R_j is the achievable rate of j^{th} UAVB-NIB with power allocation $f_j P_H$ and circuit power consumption of P_{c_2} in the backhaul. Similarly, the spectrum efficiency[6] describes the amount of data transmitted over a given spectrum with minimum transmission errors. The average SE of the BL with NOMA can be viewed as $\mathrm{SE}^b_{\mathrm{avg}} = \frac{1}{J}\sum_j R_j/B_H$, while the area SE (ASE) of the BL can be presented as:

$$\mathrm{ASE}_b = \frac{\mathrm{SE}^b_{\mathrm{avg}}}{\pi R^2}, \tag{54}$$

The described AEE and ASE of the BL between HAPS and UAVB-NIBs are analyzed for optimal versus sub-optimal resource allocation strategies in Fig. 7(c). We assume an urban area of 60km radius and 3000users/km^2 user density served by the wide-beamed UAVB-NIBs with beam radii 5km. We further assume 6.4GHz carrier frequency with 100MHz channel bandwidth for the backhaul connection. The AEE is observed for the range of transmit SNR for three different circuit power consumption scenarios i.e., $P_c = 10$W, $P_c = 20$W, and $P_c = 30$W. The lower transmit SNR values signify limited transmit power. For example, a NOMA-ASE of $5e-4$bps/Hz/km^2 is achieved at a transmit SNR of -10dB in contrast to $15e-4$bps/Hz/km^2 at a transmit SNR of 30dB. Likewise, -10dB SNR yields 70Mbps/W NOMA-AEE as compared to 88Mbps/W NOMA-AEE at 5dB SNR. This renders 66.67% decrease in NOMA-ASE and 20.45% decrease in NOMA-AEE with severe resource constraints. Evidently, the AEE of NOMA based power allocation outperforms the OFDMA counterpart for the entire range of transmit SNR. Moreover, the NOMA-AEE decreases with increasing circuit power consumption whereas the NOMA-AEE initially increases with increasing transmit SNR and then decreases with further increase in transmit SNR. This renders the maximum NOMA-AEE of 90Mbps/W around 5dB transmit SNR for all circuit power consumptions. In addition, the Fig. 7(c) reveals the ASE of the same system for three different coverage radii. Clearly, the ASE decreases with increasing coverage area as the same HAPS resources are now utilized to serve increasing number of users requiring more UAVB-NIBs with fixed beam coverage areas. Moreover, the SE increases with the increasing transmit SNR owing to the increase in the achievable rate. Lastly, the NOMA-ASE outperforms OMA-ASE for all transmit SNR and all coverage radii. For instance, NOMA-ASE renders around 20% percentage increase over conventional OMA-ASE at 20dB transmit SNR.

[5]EE is measured in bits/Joules i.e., a higher value of EE indicates the higher amount of data in bits that can be sent with minimal energy consumption.

[6]It is a measure of how efficiently a limited frequency spectrum is utilized to transmit the data by the proposed communication system. It is typically measured in bps/Hz.

E. Average Sum Rate Performance

The proposed non-uniform power allocation (NUPA) strategy is compared with the well-known water-filling power allocation (WFPA) and conventional uniform power allocation (UPA) considering the average sum rate of the AL. WFPA approach allocates more power to the users with better channels and is known to enhance the sum-rate performance and maximize the efficiency. Fig. 8(a) presents the downlink sum rate with the UAVB-NIB transmission power budget ranging from 0dBW to 16dBW for three different area configurations. Sub urban, urban, and dense urban areas are assumed to have distinct user densities i.e.,1000users/km^2, 3000users/km^2, and 5000users/km^2, respectively. In addition, they have unique environmental parameter pairs $(\eta_{\mathrm{LOS}}, \eta_{\mathrm{NLOS}})$; $(0.1, 21), (1.0, 20)$, and $(1.6, 23)$ in respective order [43]. The values of the constants are $a = 11.95$, and $b = 0.136$ [44] whereas the RAT operational demands according to the area configurations are shown in Fig. 5. We suppose maximum antenna gain of UAVB-NIBs $G_{\max} = 23$dBi, HPBW $\theta_J^{3\mathrm{dB}} = 12^o$ and transmit diversity $M = 2$, unless specified otherwise. The sum rates of LAPS-GUs downlink are averaged over numerous channel instances. Evidently, the sum rate increases with the increase in transmission power. However, the gain is particularly significant in the optimal power allocation strategy. We further observe that dense urban area exhibits highest sum rate owing to the high user-density requiring concentrated beams from a large number of UAVB-NIBs to serve the given coverage area. We can observe the percentage increase in average sum rate of upto 70% and 276.14% by using the proposed NUPA over WFPA and UPA, respectively. Moreover, we perceive the percentage decrease of upto 39.28% in average sum rates of the AL with NUPA owing to severe resource constraint (restrained transmit power).

F. Jain's fairness index

The fairness of a communication system is analyzed to determine whether all participating nodes are receiving a fair share of the system resources. The UF of the GUs in the AL can be quantified using the Jain's fairness index as:

$$\mathcal{J}_a = \frac{(\sum_{k=1}^{K} R_{kj}^{\Omega})^2}{K \cdot \sum_{k=1}^{K} {R_{kj}^{\Omega}}^2}. \tag{55}$$

The UF is evaluated for a dense urban area versus transmit SNR for varying number of transmit antennas in Fig. 8(b). The average fairness index (AFI) is the fairness index of all users in the given coverage area averaged over numerous channel instances. We investigate the AFI for the proposed PA, uniform PA, and channel inversion PA (CIPA). Channel inversion inverts the channel power gain and aims at maximizing the user fairness. However, the proposed NUPA outperforms the famous CIPA and UPA in the average fairness performance for the entire range of transmit SNR. The AFI increases with increasing transmit diversity but we observe different trends of the three power allocation schemes with respect to the transmit SNR. Increasing transmit SNR results

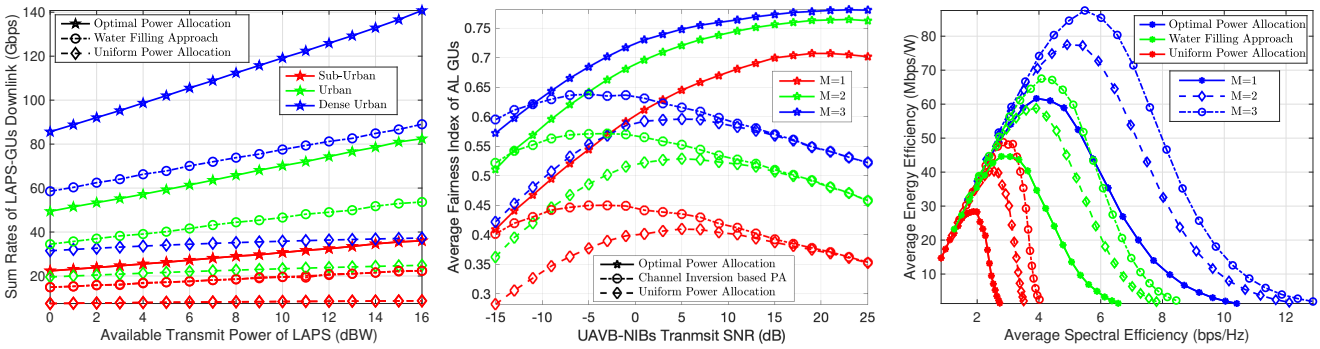

(a) Average sum rate of AL (b) Average fairness index (c) AEE and $\mathrm{SE}_{\mathrm{avg}}$ of AL

Fig. 8: Effect of optimal resource allocation on sum-rate, fairnes index, EE and SE in the AL

in increasing fairness amongst users for the NUPA, whereas it initially increases and then decreases with increasing transmit SNR for the CIPA and UPA. Interestingly, the CIPA AFI performance is equally well as NUPA for lower transmit SNR and merges to UPA for higher transmit SNR values. The CIPA and UPA demonstrate the maximum AFI at -5dB and 5dB SNR, respectively, but the maximum possible AFI values are still 18.18% and 38.4615% less than the AFI of optimal power allocation at respective SNR values with $M = 1$. Overall, we observe 61.36%, 33.33%, and 21.88% improvement in AFI using NUPA over CIPA with $M = 1, 2$, and 3 transmit antennas, respectively. Likewise, we notice 77.5%, 43.4%, and 30% percent improvement in AFI using the NUPA over UPA. The impact of severe resource constraints is quite prominent in Fig. 8(b). It reflects the AFI percentage reduction of 13.33% with reduced transmit diversity ($M = 1$ instead of $M = 3$) at 5dB transmit SNR and 30.625% with reduced transmit power for $M = 3$, respectively, in dense-urban setting employing optimal power allocation.

G. System Efficiency of the AL

The system efficiency of the AL can also be evaluated in terms of AEE and ASE. The EE metric is specifically beneficial for UAVB-NIBs operating in remote or hard-to-access areas where battery replacement or recharging may be challenging. In the AL, the AEE of the AL can be seen as the averaged EE of all the users under UAVB-NIBs coverage i.e.,

$$\mathrm{AEE_a} = \frac{1}{K}\sum_{j=1}^{J}\sum_{k}\sum_{\Omega}\frac{R_{kj}^{\Omega}}{p_{kj}^{\Omega}P_j^{\Omega}+P_{c_1}}, \qquad \forall k, \qquad (56)$$

where R_{kj}^{Ω} and p_{kj}^{Ω} are the achievable rate and power allocation factors of the concerned user in the respective order, P_j and P_{c_1} are the power budget and circuit power expenditures, respectively. Moreover, assuming the perfect CSI and RZF, we can write the average SE of the AL as:

$$\mathrm{SE}_{\mathrm{avg}}^{a} = \frac{1}{K}\sum_{j}\sum_{k}\sum_{\Omega} R_{kj}^{\Omega}/B_j^{\Omega}. \qquad (57)$$

The overall SE is averaged for all RATs as each one offers its own bandwidth to the operational set of users. The AEE versus $\mathrm{SE}_{\mathrm{avg}}^{a}$ of the AL is evaluated for the same system parameters using NUPA, WFPA, and UPA. The AEE appears to be a concave function of $\mathrm{SE}_{\mathrm{avg}}^{a}$ rendering maximum value of 86Mbits/W at 5bps/Hz for optimal power allocation, 68Mbits/W at 4bps/Hz for WFPA and 50Mbits/W at 3bps/Hz for UPA. Thus, the proposed NUPA outperforms both WFPA and UPA. Fig. 8(c) demonstrates the concentrated values on the lower-left bottom of the graph for UPA as compared to the right-top values for optimal power allocation. This signifies the lower AEE and $\mathrm{SE}_{\mathrm{avg}}^{a}$ values of UPA versus higher AEE and $\mathrm{SE}_{\mathrm{avg}}^{a}$ values of optimal power allocation for any number of transmit antennas. We can quantify the percentage improvement in the peak AEE values with optimal power allocation over the WFPA as 37.78%, 32.76%, and 29.85% for $M = 1, 2,$ and 3 transmitting UAVB-NIB antennas, respectively. Similarly, the percentage improvement of 121.43%, 92.50%, and 81.25% for $M = 1, 2,$ and 3 can achieved using NUPA as opposed to UPA, respectively.

VII. Conclusions

The compact, portable, and versatile NIB solution along with heterogeneous aerial communication platforms i.e., LAPS and HAPS can formulate an intelligent aerial wireless network. We have proposed NOMA for the backhaul connection between HAPS and UAVB-NIBS whereas zero-forcing scheme for the access MISO downlink channel between UAVB-NIBs and GUs. In addition, we have presented geometric disk cover for optimal UAVB-NIB deployment, greedy algorithm for user association, Lagrange optimization for the location optimization and successive convex approximation for the resource allocation problem in order to improve the system performance. The proposed algorithms and design guidelines enable this intelligent network to configure, deploy, and serve with the effective resource allocation, minimal power consumption, and enhanced system performance at the desired coverage area as per the users demand and QoS thresholds. Numerical results have revealed up to 50% less number of required UAVB-NIBs, 20% improvement in backhaul ASE, 275% increase in the average sum rate of the AL, and 77% improvement in average UF with the proposed strategies. The proposed system is particularly beneficial for the dynamic environments with fluctuating demands and user density. The on-demand coverage, flexible deployment, resilient operation, adaptability, and scalability makes UAVB-NIBs the ideal candidate for seamless communication services in such scenarios. They have

the ability to adjust coverage versus capacity as opposed to the fixed terrestrial communication. We can adjust the minimum target rate threshold to adapt to the users' rate requirements by allocating the requisite power. Moreover, the scalability and mobility allows us to recalculate the number of required UAVB-NIBs and their respective locations with fluctuating user density. We can limit the upperbound on beam radii to choose small beam radii and large number of UAVB-NIBs for dense population or flash crowds. An interesting future direction would be the UAVB-NIBs employment along with the existing communication infrastructure. The unpredictable interference patterns would require some sophisticated interference mitigation to ensure robust performance across diverse operational conditions.

VIII. Acknowledgment

This work is supported in part by the King Abdullah University of Science and Technology Research Funding (KRF) under Award ORA-2021-CRG10-4696. The work of Yunfei Chen is also supported by EPSRC TITAN (EP/Y037243/1, EP/X04047X/1). The work of Cheng-Xiang Wang is also supported by the National Natural Science Foundation of China (NSFC) under Grant 61960206006 and the EU H2020 RISE TESTBED2 project under Grant 872172.

Appendix A
Optimal Elevation Angle

We can write the path loss of the AL between k^{th} user and j^{th} UAVB-NIB operationg at Ω RAT as a function of the elevation angle ϕ_{jk}^{Ω} as:

$$L_{jk}^{\Omega}[\text{dB}] = \frac{A}{1+\bar{a}e^{-b\phi_{jk}^{\Omega}}} + 20\log_{10}(r_j \sec\phi_{jk}^{\Omega}) + \bar{B}^{\Omega} \quad (58)$$

where $\bar{a} = ae^{ab}$ and

$$\bar{B}^{\Omega} = 20\log_{10}\left(\frac{4\pi f_c^{\Omega}}{c}\right) + \eta_{\text{NLOS}} \quad (59)$$

Interestingly, for the worst case scenario $\phi_{jk}^{\Omega} = \phi_j$ i.e., path loss is maximum at the cell edge. Thus, solving **P1(c)** is equivalent to minimizing $L_{jk}^{\Omega}[\text{dB}]$ with respect to ϕ_j for the given r_j^* and $\mathbf{c}_j^*$. It is straight forward to prove that the path loss in (58) is convex in ϕ_j by showing that $\frac{\partial^2 L_{jk}^{\Omega}}{\partial \phi_j^2} \geq 0$. Hence, the first-order stationary point is the optimal ϕ_j^*, which can be attained by solving $\frac{\partial L_{jk}^{\Omega}}{\partial \phi_j} = 0$.

References

[1] M. Matracia, A. U. Rahman, R. Wang, M. A. Kishk, and M.-S. Alouini, "Bridging the digital divide," in *Fundam. of 6G Commun. and Netw.* Springer, 2023, pp. 113–139.

[2] W. Xu, Y. Huang, W. Wang, F. Zhu, and X. Ji, "Toward ubiquitous and intelligent 6G networks: from architecture to technology," *Sci. China Inf. Sci.*, vol. 66, no. 3, p. 130300, 2023.

[3] C.-X. Wang, Z. Lv, Y. Chen, and H. Haas, "A complete study of space-time-frequency statistical properties of the 6G pervasive channel model," *IEEE Trans. Commun.*, 2023.

[4] S. Chandrasekharan, K. Gomez, A. Al-Hourani, S. Kandeepan, T. Rasheed, L. Goratti, L. Reynaud, D. Grace, I. Bucaille, T. Wirth *et al.*, "Designing and implementing future aerial communication networks," *IEEE Commun. Mag.*, vol. 54, no. 5, pp. 26–34, 2016.

[5] C.-X. Wang, X. You, X. Gao, X. Zhu, Z. Li, C. Zhang, H. Wang, Y. Huang, Y. Chen, H. Haas *et al.*, "On the road to 6G: Visions, requirements, key technologies and testbeds," *IEEE Commun. Surveys Tuts.*, 2023.

[6] T. Zhang, C. Chen, Y. Xu, J. Loo, and W. Xu, "Joint task scheduling and multi-uav deployment for aerial computing in emergency communication networks," *Sci. China Inf. Sci.*, vol. 66, no. 9, p. 192303, 2023.

[7] H. Chang, C.-X. Wang, J. Bian, R. Feng, Y. He, Y. Chen, and E.-H. M. Aggoune, "A novel3D beam domain channel model for UAV massive MIMO communications," *IEEE Trans. Wireless Commun.*, 2023.

[8] M. Benzaghta, G. Geraci, R. Nikbakht, and D. López-Pérez, "UAV communications in integrated terrestrial and non-terrestrial networks," in *IEEE Global Commun. Conf. (GLOBECOM)*, Rio de Janeiro, Brazil, Dec. 2022, pp. 3706–3711.

[9] B. E. Y. Belmekki, A. J. Aljohani, S. A. Althubaity, A. Al Harthi, K. Bean, A. Aijaz, and M.-S. Alouini, "Cellular network from the sky: Toward people-centered smart communities," *IEEE Open J. Commun. Soc. (OJ-COMS)*, 2024.

[10] M. Wazid, A. K. Das, N. Kumar, and M. Alazab, "Designing authenticated key management scheme in 6g-enabled network in a box deployed for industrial applications," *IEEE Transactions on Industrial Informatics*, vol. 17, no. 10, pp. 7174–7184, 2020.

[11] P. P. Ray, N. Kumar, and M. Guizani, "A vision on 6G-enabled NIB: Requirements, technologies, deployments, and prospects," *IEEE Wireless Communications*, vol. 28, no. 4, pp. 120–127, 2021.

[12] M. Pozza, A. Rao, H. Flinck, and S. Tarkoma, "Network-in-a-box: A survey about on-demand flexible networks," *IEEE Commun. Surveys Tuts.*, vol. 20, no. 3, pp. 2407–2428, 2018.

[13] C.-H. Hsu, G. Manogaran, G. Srivastava, and N. Chilamkurti, "Guest editorial: 6G-enabled network in box (NIB) for industrial applications and services," *IEEE Trans. Ind. Informat.*, vol. 17, no. 10, pp. 7141–7144, 2021.

[14] A. Anjum, "Securitisation of cyber space-from prism of deterrence strategy," *Authorea Preprints*, 2023.

[15] K.-H. Park, M.-S. Alouini, and Y. Chen, "On-demand networking for ubiquitous connectivity and network resilience: A network-in-a-box solution," *arXiv preprint arXiv:2110.01726*, 2021.

[16] R. J. Sánchez, J. B. Evans, G. J. Minden, V. S. Frost, and K. S. Shanmugan, "RDRN: a rapidly deployable radio network-implementation and experience," in *IEEE Int. Conf. on Univ. Pers. Commun. Conf. Proc. (ICUPC'98)*, vol. 1, Florence, Italy, Oct. 1998, pp. 93–97.

[17] J. B. Evans, G. J. Minden, K. S. Shanmugan, G. Prescott, V. S. Frost, B. Ewy, R. Sanchez, C. Sparks, K. Malinimohan, J. Roberts *et al.*, "The rapidly deployable radio network," *IEEE J. Sel. Areas Commun.*, vol. 17, no. 4, pp. 689–703, 1999.

[18] J.-S. Huang, Y.-N. Lien, and C.-L. Hu, "Design of contingency cellular network," in *14th IEEE Asia-Pacific Netw. Op. Manag. Symp. (APNOMS)*, Seoul, Sep. 2012, pp. 1–4.

[19] K.-H. Park, M.-S. Alouini, and Y. Chen, "Network-in-a-box to provide health services in remote areas," *ITU Connect2Recover Initiative*, 2022.

[20] G. Sun, Z. Xu, H. Yu, and V. Chang, "Dynamic network function provisioning to enable network in box for industrial applications," *IEEE Trans. Ind. Informat.*, vol. 17, no. 10, pp. 7155–7164, 2020.

[21] Z. Lv, L. Qiao, and I. You, "6G-enabled network in box for internet of connected vehicles," *IEEE Trans. Intell. Transp. Syst.*, vol. 22, no. 8, pp. 5275–5282, 2020.

[22] J. Zhang, Z. Wang, D. Wang, X. Zhang, B. B. Gupta, X. Liu, and J. Ma, "A secure decentralized spatial crowdsourcing scheme for 6G-enabled network in box," *IEEE Trans. Ind. Informat.*, vol. 18, no. 9, pp. 6160–6170, 2021.

[23] D. Iland and E. M. Belding, "EmergeNet: Robust, rapidly deployable cellular networks," *IEEE Commun. Mag.*, vol. 52, no. 12, pp. 74–80, 2014.

[24] K. Heimerl, S. Hasan, K. Ali, E. Brewer, and T. Parikh, "Local, sustainable, small-scale cellular networks," in *6th Int. Conf. Inf. Commun. Tech. Dev.: Full Papers-Volume 1*, 2013, pp. 2–12.

[25] F. Hsieh, F. Jardel, E. Visotsky, F. Vook, A. Ghosh, and B. Picha, "UAV-based multi-cell HAPS communication: System design and performance evaluation," in *Proc. Global Commun. Conf. (GLOBECOM)*. Taipei, Taiwan: IEEE, Dec. 2020, pp. 1–6.

[26] C. B. Peel, B. M. Hochwald, and A. L. Swindlehurst, "A vector-perturbation technique for near-capacity multiantenna multiuser communication-part i: channel inversion and regularization," *IEEE Trans. Commun.*, vol. 53, no. 1, pp. 195–202, 2005.

[27] Y. Shibata, N. Kanazawa, M. Konishi, K. Hoshino, Y. Ohta, and A. Nagate, "System design of Gigabit HAPS mobile communications," *IEEE Access*, vol. 8, pp. 157 995–158 007, 2020.

[28] Y. Ata and M.-S. Alouini, "HAPS based FSO links performance analysis and improvement with adaptive optics correction," *IEEE Trans. Wireless Commun.*, 2022.

[29] S. Javed, M.-S. Alouini, and Z. Ding, "An interdisciplinary approach to optimal communication and flight operation of high-altitude long-endurance platforms," *IEEE Trans. Aerosp. Electron. Syst.*, 2023.

[30] G. Zheng, S. Chatzinotas, and B. Ottersten, "Generic optimization of linear precoding in multibeam satellite systems," *IEEE Trans. Wireless Commun.*, vol. 11, no. 6, pp. 2308–2320, 2012.

[31] Y. Wang, X. Fang, W. Feng, Y. Chen, N. Ge, and Z. Lu, "On-demand coverage for maritime hybrid satellite-uav-terrestrial networks," in *IEEE Int. Conf. Wirel. Commun. Signal Process. (WCSP)*, Nanjing, China, 2020, pp. 483–488.

[32] F. Hsieh and M. Rybakowski, "Propagation model for high altitude platform systems based on ray tracing simulation," in *13th IEEE Eur. Conf. Antennas Propag. (EuCAP)*, Krakow, Poland, Apr. 2019, pp. 1–5.

[33] J. L. Cuevas-Ruíz and J. A. Delgado-Penín, "Channel modeling and simulation in HAPS systems," *Eur. Wirel.*, pp. 24–27, 2004.

[34] A. G. Kanatas and A. D. Panagopoulos, *Radio wave propagation and channel modeling for earth-space systems*. CRC Press, 2017.

[35] A. A. O. OLADIPO, "Stratospheric propagation and HAPs channel modeling," *MS Thesis at Blekinge Institute of Tech., School of Eng., Department of Telecommun. Sys.*, 2007.

[36] M. Takahashi, Y. Kawamoto, N. Kato, A. Miura, and M. Toyoshima, "Adaptive power resource allocation with multi-beam directivity control in high-throughput satellite communication systems," *IEEE Wireless Commun. Lett.*, vol. 8, no. 4, pp. 1248–1251, 2019.

[37] A. S. Academy, "Space communication calculations," Jan. 2017.

[38] J. Zhang, C. Liu, X. Li, H.-L. Zhen, M. Yuan, Y. Li, and J. Yan, "A survey for solving mixed integer programming via machine learning," *Neurocomputing*, vol. 519, pp. 205–217, 2023.

[39] B. Liu, C. Jiang, L. Kuang, and J. Lu, "Joint user grouping and beamwidth optimization for satellite multicast with phased array antennas," in *IEEE Global Commun. Conf. (GLOBECOM)*, Taipei, Taiwan, Dec. 2020, pp. 1–6.

[40] A. Alkhateeb, Y.-H. Nam, M. S. Rahman, J. Zhang, and R. W. Heath, "Initial beam association in millimeter wave cellular systems: Analysis and design insights," *IEEE Trans. Wireless Commun.*, vol. 16, no. 5, pp. 2807–2821, 2017.

[41] A. Al-Hourani, S. Kandeepan, and S. Lardner, "Optimal LAP altitude for maximum coverage," *IEEE Wireless Commun. Lett.*, vol. 3, no. 6, pp. 569–572, 2014.

[42] K. Wang, Y. Liu, Z. Ding, A. Nallanathan, and M. Peng, "User association and power allocation for multi-cell non-orthogonal multiple access networks," *IEEE Trans. Wireless Commun.*, vol. 18, no. 11, pp. 5284–5298, Nov. 2019.

[43] A. Al-Hourani, S. Kandeepan, and A. Jamalipour, "Modeling air-to-ground path loss for low altitude platforms in urban environments," in *IEEE Global Commun. Conf.*, Austin, TX, USA, Dec. 2014, pp. 2898–2904.

[44] Y. Sun, Z. Ding, and X. Dai, "A user-centric cooperative scheme for UAV-assisted wireless networks in malfunction areas," *IEEE Trans. Commun.*, vol. 67, no. 12, pp. 8786–8800, 2019.

Sidrah Javed (S'16, M'21) received her Bachelor of Engineering (B.E.) degree in Electrical (Telecommunication) Engineering from the National University of Science and Technology (NUST), Pakistan, in 2012. Following her graduation, she served as a Research Engineer in the Research and Development (R&D) Department at the National Radio and Telecommunication Corporation (NRTC), Pakistan, from 2012 to 2015. Dr. Javed pursued MS/PhD from 2015 to 2021 at King Abdullah University of Science and Technology (KAUST), Saudi Arabia. In 2023, she contributed her expertise as a Research Consultant at KAUST. Currently, Dr. Javed is a Postdoctoral Research Associate in the Department of Engineering at Durham University, U.K. Her current research interests include modeling, design, and performance analysis of wireless communication systems especially satellite-aerial-terrestrial hybrid communications to eliminate digital inequality.

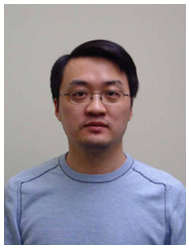

Yunfei Chen (S'02, M'06, SM'10) received his B.E. and M.E. degrees in electronics engineering from Shanghai Jiaotong University, Shanghai, P.R.China, in 1998 and 2001, respectively. He received his Ph.D. degree from the University of Alberta in 2006. He is currently working as a Reader in the School of Engineering at the University of Warwick, U.K. His research interests include wireless communications, performance analysis, joint radar communications designs, cognitive radios, wireless relaying and energy harvesting.

Mohamed-Slim Alouini (S'94, M'98, SM'03, F'09) was born in Tunis, Tunisia. He earned his Ph.D. from the California Institute ofTechnology(Caltech) in 1998 before serving as a faculty member at the University of Minnesota and later at Texas A&M University at Qatar. In 2009, he became a founding faculty member at King Abdullah University of Science and Technology (KAUST), where he currently is the Al-Khawarizmi Distinguished Professor of Electrical and Computer Engineering and the holder of the UNESCO Chair on Education to Connect the Unconnected. Dr. Alouini is a Fellow of the IEEE and OPTICA and his research interests encompass a wide array of research topics in wireless and satellite communications. He is currently particularly focusing on addressing the technical challenges associated with information and communication technologies (ICT) in underserved regions and is committed to bridging the digital divide by tackling issues related to the uneven distribution, access to, and utilization of ICT in rural, low-income, disaster-prone, and hard-to-reach areas.

Cheng-Xiang Wang (S'01, M'05, SM'08) received the B.Sc. and M.Eng. degrees in communication and information systems from Shandong University, China, in 1997 and 2000, respectively, and the Ph.D. degree in wireless communications from Aalborg University, Denmark, in 2004. He has been with Southeast University, Nanjing, China, as a professor since 2018, and he is also a professor with Pervasive Communication Research Center, Purple Mountain Laboratories, Nanjing, China. He has authored 4 books, 3 book chapters, and over 600 papers in refereed journals and conference proceedings, including 28 highly cited papers. He has also delivered 31 invited keynote speeches/talks and 18 tutorials in international conferences. His current research interests include wireless channel measurements and modeling, 6G wireless communication networks, and electromagnetic information theory. Dr. Wang is a Member of the Academia Europaea (The Academy of Europe), a Member of the European Academy of Sciences and Arts (EASA), a Fellow of the Royal Society of Edinburgh (FRSE), IEEE, IET and China Institute of Communications (CIC), an IEEE Communications Society Distinguished Lecturer in 2019 and 2020, a Highly-Cited Researcher recognized by Clarivate Analytics in 2017-2020. He is currently an Executive Editorial Committee Member of the IEEE TRANSACTIONS ON WIRELESS COMMUNICATIONS. He has served as an Editor for over ten international journals. He has served as a TPC Member, a TPC Chair, and a General Chair for more than 30 international conferences. He received 17 Best Paper Awards from international conferences.